Inorganic Chemistry

Article

pubs.acs.org/IC

Lanthanide *N,N*-Dimethylaminodiboranates as a New Class of Highly Volatile Chemical Vapor Deposition Precursors

Scott R. Daly, Do Young Kim, and Gregory S. Girolami*

The School of Chemical Sciences, University of Illinois at Urbana−Champaign, 600 South Mathews Avenue, Urbana, Illinois 61801, United States

Supporting Information

ABSTRACT: New lanthanide *N,N*-dimethylaminodiboranate (DMADB) complexes of stoichiometry $Ln(H_3BNMe_2BH_3)_3$ and $Ln(H_3BNMe_2BH_3)_3(thf)$ have been prepared, where Ln = yttrium, lanthanum, cerium, praseodymium, neodymium, samarium, gadolinium, terbium, dysprosium, holmium, erbium, thulium, and lutetium, except that isolation of the desolvated complexes proved difficult for Eu and Yb. The tetrahydrofuran (thf) complexes are all monomeric, and most of them adopt 13-coordinate structures in which each DMADB group chelates to the metal center by means of four B−H···Ln bridges (each BH_3 group is κ^2H; i.e., forms two B−H···Ln interactions). For the smallest three lanthanides, Tm, Yb, and Lu, the metal center is 12 coordinate because one of the DMADB groups chelates to the metal center by means of only three B−H···Ln bridges. The structures of the base-free $Ln(H_3BNMe_2BH_3)_3$ complexes are highly dependent on the size of the lanthanide ions: as the ionic radius decreases, the coordination number decreases from 14 (Pr) to 13 (Sm) to 12 (Dy, Y, Er). The 14-coordinate complexes are polymeric: each metal center is bound to two chelating DMADB ligands and to two "ends" of two ligands that bridge in a $Ln(\kappa^3H\text{-}H_3BNMe_2BH_3\text{-}\kappa^3H)Ln$ fashion. In the 13-coordinate complexes, all three DMADB ligands are chelating, but the metal atom is also coordinated to one hydrogen atom from an adjacent molecule. The 12-coordinate complexes adopt a dinuclear structure in which each metal center is bound to two chelating DMADB ligands and to two ends of two ligands that bridge in a $Ln(\kappa^2H\text{-}H_3BNMe_2BH_3\text{-}\kappa^2H)Ln$ fashion. The complexes react with water, and the partial hydrolysis product $[La(H_3BNMe_2BH_3)_2(OH)]_4$ adopts a structure in which the lanthanum and oxygen atoms form a distorted cube; each lanthanum atom is connected to three bridging hydroxyl groups and to two chelating DMADB ligands. One B−H bond of each chelating DMADB ligand forms a bridge to an adjacent metal center. Field ionization MS data, melting and decomposition points, thermogravimetric data, and NMR data, including an analysis of the paramagnetic lanthanide induced shifts (LIS), are reported for all of the complexes. The $Ln(H_3BNMe_2BH_3)_3$ compounds, which are highly volatile and sublime at temperatures as low as 65 °C in vacuum, are suitable for use as chemical vapor deposition (CVD) and atomic layer deposition (ALD) precursors to thin films.

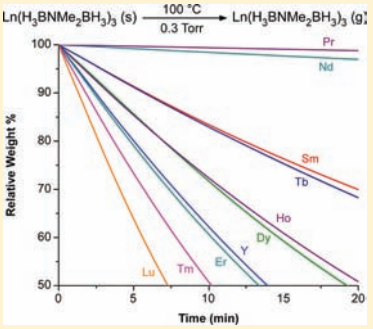

INTRODUCTION

Lanthanide materials exhibit a wide variety of fascinating electrical, optical, and magnetic properties that make them ideally suited for a diverse range of applications. Lanthanide oxides are excellent high-κ dielectrics and are constituents in superconducting materials such as $LnBa_2Cu_3O_{7-x}$.[1] Lanthanide borides exhibit unusual electronic characteristics and remarkable magnetic properties.[2] For instance, the lanthanide hexaborides (LnB_6) have high electron emissivities and are currently used as thermionic emitters in electron microscopes,[3−5] and some of the lanthanide tetraborides, LnB_4, exhibit magnetically induced phase transitions.[2] In addition, ternary boride phases with the transition metals, such as $Ln_2Fe_{14}B$, are strong permanent magnets.[6,7] Lanthanides are also commonly used as dopants to impart or enhance the properties of photonic devices[8] such as lasers,[9] electroluminescent displays,[10−14] fiber-optics,[15] light-emitting diodes,[16,17] light-emitting organic−inorganic hybrids,[18−20] and thermoelectric devices.[21]

The exponential scaling of transistors, in accordance with the semiconductor roadmap,[22] has led to the use of materials with higher dielectric constants, κ, relative to SiO_2 (κ = 3.9) to avoid significant gate leakage current as the thickness of the dielectric layer decreases. The lanthanide oxides have been suggested as next-generation dielectric barriers in metal-oxide semiconductor field-effect transistors (MOSFETS) because they have high dielectric constants, relatively large bandgaps, and high thermodynamic stablilty on silicon.[23−28] Of all the methods to deposit lanthanide oxides, chemical vapor deposition (CVD) and atomic layer deposition (ALD) are highly attractive because they can achieve uniform step coverage even in recessed features with high aspect ratios (AR > 5:1).[29,30] Physical vapor deposition (PVD), which is a line-of-sight method, will eventually be unable to coat uniformly the high AR trenches and vias that will constitute future microelectronic architectures.

Ideal CVD and ALD precursors for microelectronic applications must be volatile enough to enable conformal coverage and must react under mild conditions to afford the desired film composition. For several reasons, there are relatively few highly

Received: August 24, 2011
Published: June 11, 2012

dx.doi.org/10.1021/ic201852j | Inorg. Chem. 2012, 51, 7050−7065

volatile lanthanide-containing precursors.[31] Because lanthanides have large radii, they often form complexes that have polymeric (and thus nonvolatile) structures. Polymerization can be prevented by incorporating additional Lewis bases into the metal coordination spheres, but heating often results in dissociation of the Lewis bases (and a return to a polymeric structure) rather than sublimation. Lanthanide precursors that do have sufficient volatility for CVD and ALD applications typically employ anionic ligands that either are sterically bulky, such as silylamides,[32−36] or are multidentate (or polyhapto), such as β-diketonates,[37−44] cyclopentadienyls,[45−51] amidinates,[52−56] and guanidinates.[56−59] Neutral chelating donors (such as glymes) are often employed to fill remaining vacancies in the coordination sphere, sometimes by grafting them onto the anionic ligands. Examples of these ligand types include ether-functionalized β-ketoiminates[60,61] and alkoxides.[62−69] Several reviews of lanthanide precursors and their use in CVD and ALD have been published.[12,23,28,31,70−77]

In previous studies, we have found that monomeric borohydride complexes of group 4 and group 6 transition metals are useful as CVD precursors because they are highly volatile and have low decomposition temperatures. For instance, $Ti(BH_4)_3(dme)$,[78−80] $Zr(BH_4)_4$,[81] $Hf(BH_4)_4$,[82−86] and $Cr(B_3H_8)_2$[87−89] have all been used for the deposition of highly conformal metal diboride thin films. Unfortunately, few lanthanide(III) borohydride complexes are volatile below their respective decomposition temperatures. The 1,2-dimethoxyethane complexes of stoichiometry $Ln(BH_4)_3(dme)$ are volatile only if Ln is relatively small; thus the complexes of yttrium and the later lanthanides (Gd−Lu) sublime in the relatively high temperature range of 150−190 °C at 10^{-2} Torr.[90] Of the known tetrahydrofuran (thf) complexes of stoichiometry $Ln(BH_4)_3(thf)_3$,[91−93] only $Y(BH_4)_3(thf)_3$ is reported to be volatile, subliming at 90 °C in vacuum, but it tends to lose two thf molecules upon heating to form the salt $[Y(BH_4)_2(thf)_4][Y(BH_4)_4]$.[94] The most volatile lanthanide borohydride complexes reported to date employ the monomethylborohydride ligand, $BH_3CH_3^-$.[95] The complexes $Ln(BH_3CH_3)_3(Et_2O)$ and $Ln(BH_3CH_3)_3(thf)$, where Ln = Yb, Lu, and Ho, sublime under vacuum at 50 and 100 °C, respectively. The authors report, however, that similar complexes of the larger lanthanides, such as samarium, are not volatile. Lanthanide borohydride and monomethylborohydride complexes also form adducts with nitrogenous donors such as acetonitrile and pyridine, but the volatilities of these complexes are usually poor.[95−97]

Recently, we reported a new class of metal complexes known as the aminodiboranates. In particular (Figure 1), we have used

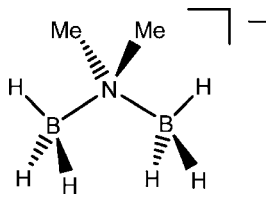

Figure 1. *N,N*-dimethylaminodiboranate (DMADB) ligand.

the *N,N*-dimethylaminodiboranate ligand, $H_3BNMe_2BH_3^-$, (DMADB)[98,99] to prepare complexes of transition metals, alkaline earths, and the actinides, many of which are highly volatile.[100−104] The DMADB ligand typically chelates to metal centers through four B−H···M bridges, so that it occupies more of the coordination sphere than the smaller borohydrides BH_4^- and $BH_3CH_3^-$. As we will show below, in some cases the DMADB ligand can bridge between metals, a feature also characteristic of the BH_4^- ligand.[105−107] Several metal DMADB complexes have already been shown to serve as excellent CVD precursors. For example, $Ti(H_3BNMe_2BH_3)_2$ affords high-quality TiB_2 films, and $Mg(H_3BNMe_2BH_3)_2$ reacts with water under CVD conditions to form highly conformal MgO.[100,108]

These results prompted us to explore the chemistry of lanthanide DMADB complexes; such species could serve as excellent precursors for the deposition of lanthanide borides or lanthanide oxides by CVD or ALD. We now report the synthesis, characterization, and volatilities of lanthanide DMADB complexes (Table 1). Portions of this work, including preliminary CVD results, have been previously reported.[109]

Table 1. Numbering Scheme for Ln DMADB Complexes

lanthanide	$Ln(H_3BNMe_2BH_3)_3(thf)$	$Ln(H_3BNMe_2BH_3)_3$
Y	**1a**	**1b**
La	**2a**	**2b**
Ce	**3a**	**3b**
Pr	**4a**	**4b**
Nd	**5a**	**5b**
Sm	**6a**	**6b**
Eu	**7a**	**7b**
Gd	**8a**	**8b**
Tb	**9a**	**9b**
Dy	**10a**	**10b**
Ho	**11a**	**11b**
Er	**12a**	**12b**
Tm	**13a**	**13b**
Yb	**14a**	**14b**
Lu	**15a**	**15b**

RESULTS AND DISCUSSION

Synthesis and Characterization of $Ln(H_3BNMe_2BH_3)_3(thf)$ Complexes. For almost all of the lanthanides (Y, Pr−Nd, Sm−Lu), treatment of the anhydrous lanthanide(III) chloride, $LnCl_3$, with 3 equiv of $Na(H_3BNMe_2BH_3)$ in thf readily affords the new complexes $Ln(H_3BNMe_2BH_3)_3(thf)$.

$$LnCl_3 + 3Na(H_3BNMe_2BH_3) \xrightarrow{thf} Ln(H_3BNMe_2BH_3)_3(thf) + 3NaCl \quad (Ln=Y, Pr−Nd, Sm−Lu)$$

These compounds can be isolated by extraction and crystallization from pentane in good yields (51−71%). By means of this method, however, we have been unable to prepare the corresponding lanthanum complex, $La(H_3BNMe_2BH_3)_3(thf)$ (**2a**), and we obtain the cerium analogue $Ce(H_3BNMe_2BH_3)_3(thf)$ (**3a**) only in low yield (<13%). The reactions of $LaCl_3$ and $CeCl_3$ with Na(DMADB) in thf give little or no pentane-extractable product, and only $LaCl_3(thf)_x$ has been recovered from the lanthanum reaction. Fortunately, **2a** and **3a** can be prepared from the corresponding LnI_3 starting material in place of the chloride.

$$LnI_3 + 3Na(H_3BNMe_2BH_3) \xrightarrow{thf} Ln(H_3BNMe_2BH_3)_3(thf) + 3NaI \quad (Ln=La, Ce)$$

The La and Ce complexes can also be prepared by adding thf to the base-free compounds $La(H_3BNMe_2BH_3)_3$ (**2b**) and $Ce(H_3BNMe_2BH_3)_3$ (**3b**), which we will describe below.

X-ray diffraction (XRD) studies of crystals obtained from pentane reveal that the $Ln(H_3BNMe_2BH_3)_3(thf)$ complexes for Y (**1a**), Nd (**5a**), Sm (**6a**), Eu (**7a**), Gd (**8a**), Dy (**10a**), and Er

dx.doi.org/10.1021/ic201852j | Inorg. Chem. 2012, 51, 7050−7065

(**12a**) are isomorphous and crystallize in the orthorhombic space group $Pca2_1$. The La complex **2a** crystallizes in the cubic space group $I23$ (Supporting Information, Table S1) but, despite this difference, its structure is similar to those of the others; an ORTEP view of a representative example is given in Figure 2. Of all the lanthanides, La has the largest radius in the

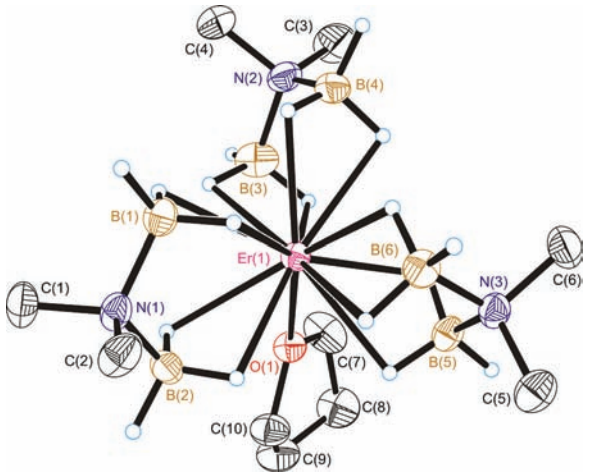

Figure 2. Molecular structure of $Er(H_3BNMe_2BH_3)_3(thf)$, **12a**. Ellipsoids are drawn at the 35% probability level, except for the hydrogen atoms, which are represented as arbitrarily sized spheres. Methyl and methylene hydrogen atoms have been deleted for clarity.

+3 oxidation state, and thus it is not entirely surprising that it crystallizes somewhat differently. In most cases, the hydrogen atoms attached to boron surfaced in the difference maps, and their locations could be refined, although sometimes with light constraints on the B−H distances. Each $H_3BNMe_2BH_3$ group chelates to the metal center by means of four B−H···Ln bridges in which each BH_3 group is κ^2H (i.e., forms two B−H···Ln interactions).

The $Ln(H_3BNMe_2BH_3)_3(thf)$ complexes of Y and La−Er are formally 13-coordinate (12 hydrogen atoms and one oxygen atom), but their structures are more conveniently described by the arrangement of the six boron atoms and the thf oxygen, which define a polyhedron that is best described as a capped octahedron with the thf ligand in the capping site.[110] The three DMADB ligands are related by a 3-fold rotational axis coincident with the M−O bond of the coordinated thf molecule. The mean lanthanide-boron and lanthanide-oxygen distances decrease across the period, as expected from the corresponding decrease in ionic radii (Table 2). Although the effect is small, the B−N−B angle of the DMADB ligand appears to decrease with the decreasing size of the lanthanide ion. For example, the B−N−B angle is 109.9(7)° for the La complex **2a** but 107.0(7)° for the Er complex **12a**. This trend, if real, is consistent with the expectation that the B−N−B angle should open up slightly if the metal is large, and close down slightly if the metal is small.

Initially, we assumed that the $Ln(H_3BNMe_2BH_3)_3(thf)$ complexes of the late lanthanides Tm, Yb, and Lu would have the same 13-coordinate structures. However, analysis of the paramagnetic lanthanide induced shifts (see below) suggested that the structures of the Tm and Yb complexes were different in some way. Single-crystal XRD studies of $Tm(H_3BNMe_2BH_3)_3(thf)$ (**13a**) and $Lu(H_3BNMe_2BH_3)_3(thf)$ (**15a**) revealed that the structures are indeed different from those of the other $Ln(H_3BNMe_2BH_3)_3(thf)$ complexes: one Ln···B distance is ~0.3−0.4 Å longer than the other five (Table 3).

Table 3. Selected Atomic Distances and Angles for $Tm(H_3BNMe_2BH_3)_3(thf)$ and $Lu(H_3BNMe_2BH_3)_3(thf)$

	Tm (**13a**)	Lu (**15a**)
	Atomic Distances (Å)	
Ln−O1	2.343(2)	2.328(3)
Ln−B1	2.727(3)	2.770(5)
Ln−B2	2.827(3)	2.729(5)
Ln−B3	2.746(3)	2.699(5)
Ln−B4	2.786(3)	2.826(5)
Ln−B5	2.733(3)	2.728(5)
Ln−B6	3.136(3)	3.139(5)
	Bond Angles (deg)	
B1−N1−B2	106.8(2)	107.7(3)
B3−N2−B4	108.2(2)	106.7(3)
B5−N3−B6	108.3(2)	108.1(3)

Refinement of the hydride positions shows that this BH_3 unit is in fact bound to the metal atom by means of one hydrogen bridge instead of two (Figure 3). As a result, these complexes have coordination numbers of 12 (11 hydrogen atoms and one oxygen atom) rather than 13.

The IR spectra of all of the $Ln(H_3BNMe_2BH_3)_3(thf)$ complexes are essentially identical. A representative complex, $Nd(H_3BNMe_2BH_3)_3(thf)$ (**5a**), exhibits two stretching bands for the terminal B−H bonds at 2392 and 2342 cm^{-1} and five distinct stretching bands for the bridging B−H bonds at 2285, 2252, 2216, 2173, and 2066 cm^{-1} (Figure 4). Of the bands due to the bridging B−H bonds, the most intense are at 2392, 2216, and 2173 cm^{-1}; over the entire lanthanide period, the frequencies of these three strong B−H bands vary slightly: from 2390−2420, from 2213−2230, and from 2168−2191 cm^{-1}, respectively. The frequencies of these intense bands are similar to those observed for the uranium analogue $U(H_3BNMe_2BH_3)_3(thf)$, as shown in Figure 4.[104] Two diagnostic peaks corresponding to the symmetric C−O−C stretch of the coordinated thf molecule are clearly observed in most of the IR spectra between 856 and 837 cm^{-1}.[111,112] The asymmetric C−O−C stretch is obscured by other peaks in the spectrum.

Table 2. Average Atomic Distances and Angles for $Ln(H_3BNMe_2BH_3)_3(thf)$ Complexes

	Y (**1a**)	La (**2a**)	Nd (**5a**)	Sm (**6a**)	Eu (**7a**)	Gd (**8a**)	Dy (**10a**)	Er (**12a**)
				Mean Atomic Distances (Å)				
Ln−B	2.82(5)	2.94(2)	2.88(2)	2.85(2)	2.85(3)	2.84(3)	2.82(4)	2.80(5)
Ln−O	2.436(8)	2.513(12)	2.504(7)	2.48(1)	2.48(1)	2.468(6)	2.447(3)	2.423(8)
				Mean Bond Angles (deg)				
B−N−B	107.9(7)	109.9(7)	108.7(5)	108.3(4)	108(1)	107.9(6)	107.6(6)	107.0(8)
B−Ln−B	53.4(3)	51.3(3)	52.7(3)	52.97(8)	53.2(3)	53.1(1)	53.6(3)	53.7(1)

dx.doi.org/10.1021/ic201852j | Inorg. Chem. 2012, 51, 7050−7065

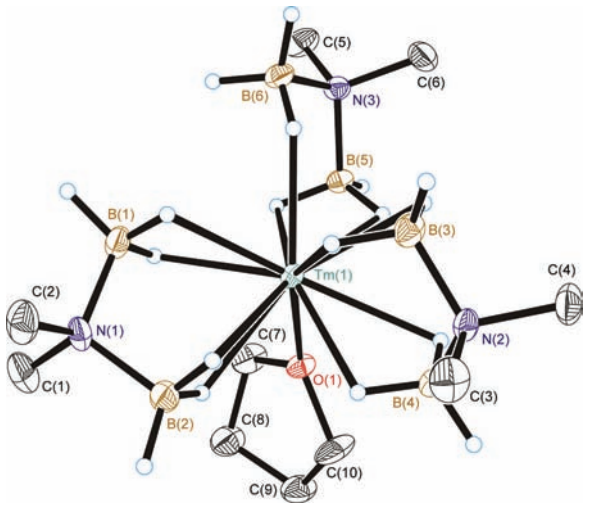

Figure 3. Molecular structure of $Tm(H_3BNMe_2BH_3)_3(thf)$, **13a**. Ellipsoids are drawn at the 35% probability level, except for the hydrogen atoms, which are represented as arbitrarily sized spheres. Methyl and methylene hydrogen atoms have been deleted for clarity.

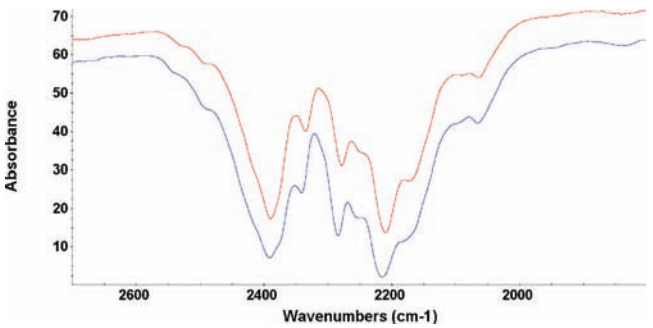

Figure 4. B–H stretching region of the IR spectrum of Nd$(H_3BNMe_2BH_3)_3(thf)$, **5a**, (bottom, blue) and U$(H_3BNMe_2BH_3)_3(thf)$ (top, red).[104]

The ^1H NMR spectra in C_6D_6 of the diamagnetic species Y$(H_3BNMe_2BH_3)_3(thf)$ (**1a**), La$(H_3BNMe_2BH_3)_3(thf)$ (**2a**), and Lu$(H_3BNMe_2BH_3)_3(thf)$ (**14a**) are very similar. The NMe_2 group is a singlet (δ 2.24–2.30), and the bound thf molecule exhibits multiplets for the α (δ 3.78–3.83) and β (δ 1.13–1.21) protons. A very broad 1:1:1:1 quartet is also observed at δ 2.51–3.05 in each spectrum; this resonance is due to the BH_3 protons, which are coupled to the quadripolar ^{11}B nuclei (I = 3/2) (Table 4). The ^{11}B NMR spectra of these species feature binomial quartets due to coupling to the three equivalent BH_3 hydrogen atoms. Thus, exchange of the terminal and bridging hydrogens is rapid on the NMR time scale at room temperature, as is typical of most borohydride complexes.[105] The ^{11}B NMR chemical shifts become slightly more shielded as the size of the metal center decreases: δ −2.9 for the La^{3+} compound **2a** (r_{ionic} = 1.032 Å), δ −5.7 for the Y^{3+} compound **1a** (r_{ionic} = 0.900 Å), and δ −6.4 for the Lu^{3+} compound **14a** (r_{ionic} = 0.861 Å).[113] A similar trend is observed for the ^1H NMR shifts. NMR data for the paramagnetic lanthanide species will be discussed below.

The dominant ions in the positive-ion field ionization (FI) mass spectra of the Ln$(H_3BNMe_2BH_3)_3(thf)$ complexes (Table 5) are formed by loss of thf or one DMADB anion. Predominant among these species is $Ln(H_3BNMe_2BH_3)_3^+$, and most of the spectra also contain peaks due to $Ln(H_3BNMe_2BH_3)_2^+$ and $Ln_2(H_3BNMe_2BH_3)_5^+$ ions, the latter presumably arising by loss of thf and subsequent dimerization. In some of the spectra, small peaks due to the thf-containing species $Ln(H_3BNMe_2BH_3)_3(thf)^+$ and $Ln_2(H_3BNMe_2BH_3)_5(thf)^+$ can also be seen; the low relative abundances suggest that the thf molecule is easily dissociated upon ionization. Assignment of stoichiometries to the masses seen requires some care because thf and $H_3BNMe_2BH_3^-$ both have masses near 72 amu. Comparison of these fragments to analgous fragments in the FI mass spectra of the Ln$(H_3BNMe_2BH_3)_3$ complexes (see below) confirms that thf-containing species as well as thf-free species are both generated upon electron impact. In contrast, the ionized fragments for the Ln$(H_3BNMe_2BH_3)_3$ complexes, which have no thf present, have peak envelopes identical to those calculated for the thf-free fragments.

Table 4. ^1H and ^{11}B NMR Resonances of Ln$(H_3BNMe_2BH_3)_3(thf)$ Complexes[a]

Ln	NMe_2	α-thf	β-thf	BH_3	^{11}B
Y	2.28	3.83	1.18	2.51	−5.7
La	2.30	3.78	1.13	2.87	−2.9
Ce	0.79	7.11	3.84	20.39	23.1
Pr	0.02	9.93	6.48	58.06	75.1
Nd	3.06	0.66	0.95	82.86	104.8
Sm	2.25	3.80	1.29	−1.86	−9.8
Eu					−176.8
Gd					
Tb	−27.47	95.57	54.49		−556.3
Dy	−22.72	94.84	59.71		−428.4
Ho	11.46	−1.80	2.05		−269.4
Er	14.79	−43.14	−28.57		−171.5
Tm[b]	−6.60	−17.86	−17.86	−92.87	−133.0
Yb	−0.26	1.15	3.48	−18.72	−47.4
Lu	2.24	3.80	1.21	3.05	−6.4

[a]Blank entries indicate resonances that could not be located in the spectra. [b]The thf resonances for Tm overlap, which was verified by VT ^1H NMR studies (Supporting Information, Figure S1).

The melting points of the Ln$(H_3BNMe_2BH_3)_3(thf)$ complexes are essentially identical for La through Sm (132–137 °C) but then steadily decrease from Gd (128–129 °C) to Lu (99–101 °C). The complexes Eu$(H_3BNMe_2BH_3)_3(thf)$ and Yb$(H_3BNMe_2BH_3)_3(thf)$ decompose rather than melt, and evolve gas as the solid liquefies. This behavior is likely a consequence of thermally induced reduction of Eu^{3+} and Yb^{3+} to their corresponding divalent oxidation states, as has been observed for trivalent europium and ytterbium tetrahydroborate complexes.[114] The Eu^{2+} and Yb^{2+} complexes M$(H_3BNMe_2BH_3)_2(thf)_2$ can in fact be isolated; the synthesis and characterization of these divalent lanthanide aminodiboranate complexes has been described previously.[115]

Synthesis and Characterization of Ln$(H_3BNMe_2BH_3)_3$ Complexes. Grinding anhydrous $LnCl_3$ with 3 equiv of Na(DMADB) in the absence of solvent produces the corresponding base-free Ln$(H_3BNMe_2BH_3)_3$ complexes, which can be isolated by sublimation under vacuum. The volatility of these complexes at 10^{-2} Torr increases across the period: La$(H_3BNMe_2BH_3)_3$ (**2b**) sublimes at 125 °C, whereas Lu$(H_3BNMe_2BH_3)_3$ (**15b**) sublimes at the remarkably low temperature of 65 °C. The yields are typically low (<33%) and

dx.doi.org/10.1021/ic201852j | Inorg. Chem. 2012, 51, 7050–7065

Table 5. Major Fragments, and Those Containing thf, Observed in the FI Mass Spectra of $Ln(H_3BNMe_2BH_3)_3(thf)$ Complexes

	ML_2^+		$^aML_3^+$		$ML_3(thf)^+$		$M_2L_5^+$		$M_2L_5(thf)^+$	
M	mass (m/z)	rel. int. (%)	mass (m/z)	rel. int. (%)	mass (m/z)	rel. int. (%)	mass (m/z)	rel. int. (%)	mass (m/z)	rel. int. (%)
La (**2a**)	283	25	353	100			636	30		
Ce (**3a**)			355	15	414	2	640	5	710	2
Pr (**4a**)			355	40			642	15		
Nd (**5a**)	286	15	358	100			645	60	718	15
Sm (**6a**)	296	60	362	100			606	80	732	5
Eu (**7a**)	295	40	367	75			663	15		
Gd (**8a**)	301	3	379	25			674	5		
Tb (**9a**)	303	5	373	15			676	5		
Dy (**10a**)			377	95			684	100		
Ho (**11a**)	308	30	380	70			688	100	760	10
Y^b (**1a**)	233	40	303	100	376	6	538	40	608	15
Er (**12a**)			381	5						
Tm (**13a**)	312	100	383	80			697	65		
Yb (**14a**)	316	45	388	100			704	65		
Lu (**15a**)	319	20	389	30			709	100		

$^aML_3^+$ fragments are mixtures of $Ln(H_3BNMe_2BH_3)_3^+$ and $M(H_3BNMe_2BH_3)_2(thf)^+$. ^{b}Yttrium placed in the series according to its ionic radii; L = $H_3BNMe_2BH_3^-$.

are somewhat variable by this preparative method.

$$LnCl_3 + 3Na(H_3BNMe_2BH_3) \xrightarrow{\text{grinding}} Ln(H_3BNMe_2BH_3)_3 + 3NaCl$$

Fortunately, sublimation of the thf adducts $Ln(H_3BNMe_2BH_3)_3(thf)$ under dynamic vacuum results in the loss of thf to produce the corresponding $Ln(H_3BNMe_2BH_3)_3$ species in high yields. Thus, whereas the ^1H NMR spectrum of $Er(H_3BNMe_2BH_3)_3(thf)$ (**12a**) exhibits resonances due to the coordinated thf ligand at δ −43.14 (OCH_2) and δ −28.57 (β-CH_2) and a singlet for the NMe_2 protons at δ 14.79, sublimation of this material under a dynamic vacuum affords a product that shows no thf resonances and only a single peak at δ −32.50 for the NMe_2 protons of $Er(H_3BNMe_2BH_3)_3$ (**12b**) (Figure 5). Desolvation also causes the ^{11}B NMR resonance to move from δ −171.5 in **12a** to δ −324.4 for **12b**.

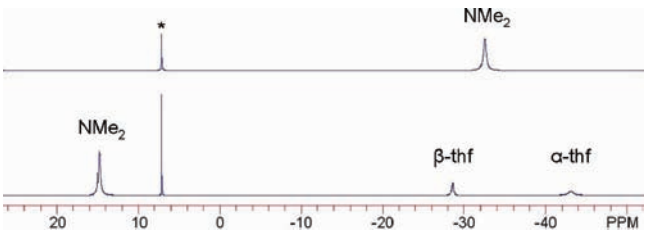

Figure 5. ^1H NMR spectra (C_6D_6, 20 °C) of $Er(H_3BNMe_2BH_3)_3(thf)$ (**12a**, bottom) and $Er(H_3BNMe_2BH_3)_3$ (**12b**, top) obtained by sublimation of **12a**. The asterisk denotes the deuterobenzene solvent resonance.

Neither the solid state method nor the thf desolvation method works particularly well to afford the $Ln(H_3BNMe_2BH_3)_3$ complexes of Eu and Yb. The DMADB complexes of both of these lanthanides reduce readily to their corresponding divalent analogues when heated, although sublimation of $Eu(H_3BNMe_2BH_3)_3(thf)$ under relatively mild conditions (T < 80 °C) affords a solid of which the base free compound appears to be a component.

Single crystal XRD studies of the base-free $Ln(H_3BNMe_2BH_3)_3$ complexes reveal that their structures are strongly dependent on the ionic radius of the lanthanide ion, with the coordination number decreasing as the radius decreases across the period. As for the thf adducts, hydrogen atoms attached to boron surfaced in most of the difference maps, and their positions could be refined.

$Pr(H_3BNMe_2BH_3)_3$ (**4b**) adopts a polymeric structure in which each metal center is surrounded by two chelating DMADB ligands and two ligands that bridge between metal centers in a $Pr(\kappa^3\text{-}H_3BNMe_2BH_3\text{-}\kappa^3)Pr$ fashion. The total coordination number is 14 for each metal center (Figure 6).

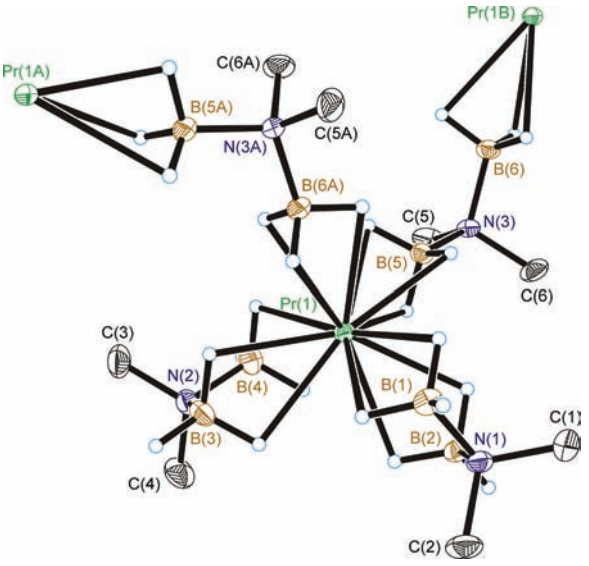

Figure 6. Molecular structure of $Pr(H_3BNMe_2BH_3)_3$, **4b**. Ellipsoids are drawn at the 35% probability level, except for the hydrogen atoms, which are represented as arbitrarily sized spheres. Methyl hydrogen atoms have been deleted for clarity.

For the chelating DMADB ligands, in which each BH_3 unit is bound κ^2, the Pr···B distances range from 2.855(4)−2.891(4) Å. In contrast, for the bridging DMADB ligands, in which the BH_3 groups coordinate to the metal in a κ^3 fashion, the Pr···B distances are much shorter: 2.656(4) and 2.671(4) Å. For comparison, the Pr···B distances to the κ^3-BH_4 groups in the

dx.doi.org/10.1021/ic201852j | Inorg. Chem. 2012, 51, 7050−7065

methoxyethyl-substituted cyclopentadienyl complex $(MeOCH_2CH_2C_5H_4)_2Pr(BH_4)$ and several heteroleptic β-diketiminato-borohydride complexes range from 2.644(8) to 2.757(18) Å.[116,117] A complex with a Pr···B distance of 2.824(5) Å is claimed to involve a κ^3-BH_4 group, but the present results suggest that this distance is to a κ^2 group instead.[117] The structure of **4b** is the same as that of the $U(H_3BNMe_2BH_3)_3$ isomer grown from toluene;[103] the isomorphous nature of the Pr and U compounds is not surprising in view of the similar ionic radii: 0.99 Å for Pr^{3+} and 1.025 for U^{3+}.[113] The Pr···B distances in **4b** are very similar to the U···B distances in $U(H_3BNMe_2BH_3)_3$ of 2.861(7)−2.902(6) for the κ^2 interactions, and 2.665(6) and 2.670(6) Å for the κ^3 interactions.

$Sm(H_3BNMe_2BH_3)_3$ (**6b**), which contains the smaller Sm^{3+} ion (r_{ionic} = 0.96 Å),[113] adopts a different polymeric structure in which the three DMADB ligands all chelate to the metal center in the usual fashion. The Sm···B distances of 2.783(4)−2.870(4) Å for these κ^2-BH_3 interactions are, as expected, significantly longer than the κ^3 interactions of 2.579(3) to 2.680(5) Å seen for certain samarium borohydride complexes.[118−122] The samarium ion in **6b** is located 0.32 Å out of the plane of the three nitrogen atoms, which opens up a thirteenth coordination site that is occupied by an intermolecular Sm···H−B bridge from an adjacent molecule (Figure 7).

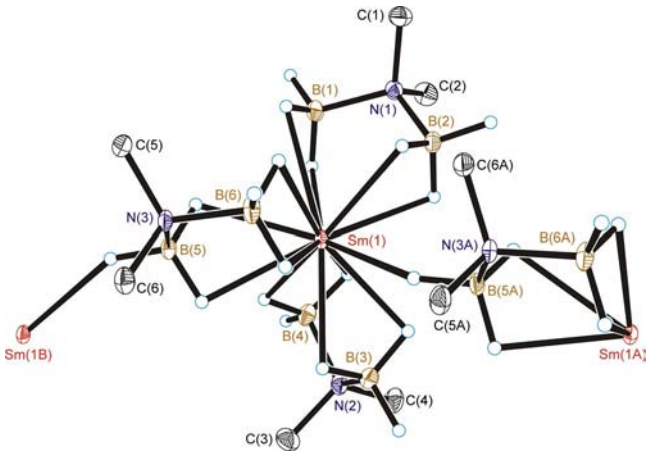

Figure 7. Molecular structure of $Sm(H_3BNMe_2BH_3)_3$, **6b**. Ellipsoids are drawn at the 35% probability level, except for the hydrogen atoms, which are represented as arbitrarily sized spheres. Methyl hydrogen atoms have been deleted for clarity.

The intermolecular Sm−H distance of 2.50 Å is similar to the average intramolecular Sm−H distance of 2.44 Å. The 13-coordinate structure of **6b** matches the structural isomer of $U(H_3BNMe_2BH_3)_3$ grown from pentane, in which the uranium atom is also displaced, by 0.30 Å, out of the plane of the nitrogen atoms and forms one intermolecular U−H contact.[103]

The DMADB complexes of Dy^{3+} (**10b**), Y^{3+} (**1b**), and Er^{3+} (**12b**), which have even smaller ionic radii of 0.912, 0.900, and 0.890 Å, respectively,[113] adopt dinuclear structures (Figure 8). Each metal center bears two chelating DMADB ligands and two DMADB ligands that bridge between the two metals. The connectivity of each bridging ligand is $Ln(\kappa^2$-$H_3BNMe_2BH_3$-$\kappa^2)Ln$, making these complexes formally 12-coordinate. The average B−N−B bond angles of 109.0−109.3° for the chelating DMADB ligands are smaller than the 112.9, 111.3, and 113.4° angles seen for the bridging ligands in **1b**, **10b**, and **12b**, respectively.

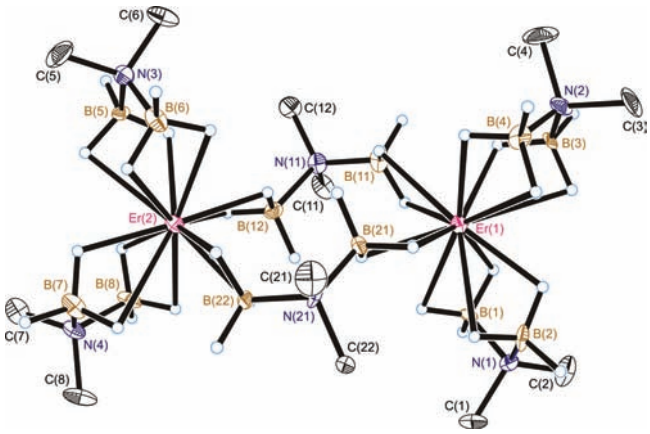

Figure 8. Molecular structure of $Er(H_3BNMe_2BH_3)_3$, **12b**. Ellipsoids are drawn at the 35% probability level, except for the hydrogen atoms, which are represented as arbitrarily sized spheres. Methyl hydrogen atoms have been deleted for clarity.

Despite the fact that all the Ln···B interactions in **10b**, **1b**, and **12b** are κ^2, the Ln···B distances in these compounds vary significantly: 2.687(10)−2.838(12) Å for **10b**, 2.672(7)−2.853(7) Å for **1b**, and 2.590(17)−2.849(19) Å for **12b** (Table 6). Most likely, the variations reflect differences in the local interligand repulsions, and comparisons with other complexes show that even the shortest of these distances is longer than expected for a κ^3 interaction. For example, Y···B distances reported for κ^2-BH_4^- groups of 2.693(8) to 2.836(1) Å[116,123−126] are similar to those observed in **1b**, whereas Y···B distances for κ^3-BH_4^- groups are significantly shorter at 2.485(3)−2.584(3) Å.[124,127,128] Few structurally characterized dysprosium and erbium borohydride complexes are known, but the data again are consistent with our findings: the Ln···B distances for the κ^2-borohydride in $(Cp^{ttt})_2Dy(BH_4)$ is 2.660(4) Å whereas those for the κ^3-borohydrides in $(2,4,6\text{-}t\text{-}Bu\text{-}C_6H_2O)Er(BH_4)_2(thf)_2$ and $[(Me_3Si)_2NC(NCy)_2]Ln(BH_4)_2(thf)_2$ are 2.483(8) and 2.559(4) Å, respectively.[129,130]

As seen for the diamagnetic $Ln(H_3BNMe_2BH_3)_3(thf)$ complexes, the solution ^1H and ^{11}B NMR spectra of the diamagnetic $Ln(H_3BNMe_2BH_3)_3$ species **1b**, **2b**, and **15b** are readily interpretable (Table 7). Only one ^1H NMR signal is observed for the NMe_2 and BH_3 groups for these complexes at room temperature, and no decoalescence is observed upon cooling the samples to −70 °C. Because **1b** (and presumably also **15b**) adopts a dinuclear structure in the solid state with multiple NMe_2 and BH_3 environments, either the complexes are monomeric in solution or they remain dinuclear but undergo dynamic processes that exchange the different sites.

Despite the differences in DMADB coordination modes, the solid state IR spectra of the $Ln(H_3BNMe_2BH_3)_3$ complexes in the B−H stretch region are similar to those of their $Ln(H_3BNMe_2BH_3)_3(thf)$ counterparts. The two thf bands at 856 and 837 cm^{-1} seen for the $Ln(H_3BNMe_2BH_3)_3(thf)$ complexes are not present in the IR spectra of the base-free compounds, as expected.

The field ionization mass spectra of the $Ln(H_3BNMe_2BH_3)_3$ complexes are also similar to those observed for their $Ln(H_3BNMe_2BH_3)_3(thf)$ analogues, except for the absence of thf-containing species (Table 8). Peaks corresponding to the ion $Ln(H_3BNMe_2BH_3)_3^+$ and the dinuclear species $Ln_2(H_3BNMe_2BH_3)_5^+$ can be observed in all of the spectra, and the fragment $Ln(H_3BNMe_2BH_3)_2^+$ is evident for all but

dx.doi.org/10.1021/ic201852j | Inorg. Chem. 2012, 51, 7050−7065

Table 6. Selected Atomic Distances and Angles for $Ln(H_3BNMe_2BH_3)_3$ Complexes

	Y (**1b**)	Pr (**4b**)	Sm (**6b**)	Dy (**10a**)	Er (**12b**)
			Atomic Distances (Å)		
Ln−B1	2.701(7)	2.867(2)	2.849(4)	2.725(10)	2.733(19)
Ln−B2	2.739(7)	2.893(2)	2.782(3)	2.734(14)	2.745(18)
Ln−B3	2.718(7)	2.890(3)	2.785(4)	2.758(13)	2.744(16)
Ln−B4	2.756(7)	2.859(3)	2.812(4)	2.699(11)	2.71(2)
Ln−B5	2.719(8)	2.671(2)	2.869(3)	2.723(10)	2.735(18)
Ln−B6	2.763(7)	2.661(2)	2.839(3)	2.747(12)	2.730(19)
Ln−B7	2.732(7)			2.738(14)	2.733(17)
Ln−B8	2.717(7)			2.723(10)	2.68(2)
Ln−B11	2.837(7)			2.687(10)	2.849(19)
Ln−B12	2.672(7)			2.837(11)	2.590(17)
Ln−B21	2.734(7)			2.838(12)	2.719(18)
Ln−B22	2.853(7)			2.725(10)	2.849(17)
			Bond Angles (deg)		
B1−N1−B2	107.3(10)	109.69(16)	109.5(2)	107.9(11)	109.6(13)
B3−N2−B4	110.8(9)	109.74(17)	108.5(2)	110.8(9)	110.4(13)
B5−N3−B6	108.4(9)	112.63(17)	108.2(2)	108.4(9)	109.0(13)
B7−N4−B8	110.2(9)			110.2(9)	107.5(13)
B11−N11−B12	113.2(10)			113.2(10)	111.5(13)
B21−N21−B22	109.4(8)			109.4(8)	115.5(12)

Table 7. ^1H and ^{11}B NMR Resonances of $Ln(H_3BNMe_2BH_3)_3$ Complexes[a]

	NMe_2	BH_3	^{11}B
Y	2.12	2.49	−5.1
La	2.22	2.78	−2.8
Ce	4.23	26.39	39.8
Pr	5.13	68.41	103.9
Nd	4.66	86.84	125.3
Sm	3.89	−4.85	−10.8
Eu			−221.6
Gd			
Tb	118.77		−343.8
Dy	94.43		−269.1
Ho	63.61		−216.5
Er	−32.50		−324.4
Tm	−116.02		−416.8
Lu	2.10	3.19	−6.3

[a]Blank entries indicate resonances that could not be located in the spectra.

10b (Dy) and **12b** (Er). For the early lanthanides (La−Tb), a peak for the trinuclear species $Ln_3(H_3BNMe_2BH_3)_8^+$ is also present; the largest relative abundance (80%) is seen for **2b** (La), suggesting that these larger clusters are favored for metals with the largest radii.

All of the $Ln(H_3BNMe_2BH_3)_3$ complexes decompose rather than melt: the solids change color irreversibly when strongly heated, and colorless (presumably organic) crystals deposit in the cooler parts of the sealed capillaries. For example, at 185 °C $Pr(H_3BNMe_2BH_3)_3$ (**4b**) changes color from light green to orange. The decomposition temperatures are similar for La through Pr (183−185 °C) but then steadily decrease across the period from Nd ($T_{dec.}$ = 176 °C) to Lu ($T_{dec.}$ = 147 °C), similar to the melting point trend observed for the $Ln(H_3BNMe_2BH_3)_3(thf)$ complexes.

NMR Spectra of the Paramagnetic Lanthanide DMADB Complexes. The large NMR frequency shifts induced by paramagnetic lanthanide ions have been well documented and remain of great interest.[131] This behavior is known as the lanthanide induced shift (LIS) and is defined as the difference in the chemical shift of a nucleus in the presence of a paramagnetic lanthanide ion (Ce^{3+}, Pr^{3+}, etc.) relative to the shift observed in the presence of a diamagnetic analogue (Y^{3+}, La^{3+}, or Lu^{3+}). The direction and magnitude of the LIS depends on the paramagnetism of the lanthanide ion and the spatial location of the nucleus with respect to the metal center and the magnetic susceptibility tensor.

The LIS is embodied in the parameter $\Delta_{a,i}$, in which the index a refers to the nucleus whose NMR shift is being measured and the index i refers to the identity of the lanthanide ion. The magnitude of $\Delta_{a,i}$ is the result of two contributions: the Fermi contact shift (δ_c), which arises from through-bond interactions, and the pseudocontact shift (δ_{pc}), which arises from through-space dipolar interactions.[132] The contact shift contribution is the product of a contact shift factor F_a, which is proportional to the electron−nuclear hyperfine coupling constant, and the electron-spin expectation value of the lanthanide ion ($\langle S_z \rangle_i$). The pseudocontact shift contribution in the general case is given by a relatively complicated expression, but the expression is greatly simplified for systems with axial symmetry (i.e., at least a 3-fold principal rotation axis). Under these circumstances, the pseudocontact shift contribution is given by the product of the magnetic constant of the lanthanide (D_i), a crystal field parameter (B_0^2), and a geometric factor (G_a) equal to $(3\cos^2\theta - 1)/r^3$, where r is the distance of the nucleus from the metal center and θ is the angle between the vector $\mathbf{r}$ and the principal axis of symmetry. These relationships are summarized in eq 1.

$$\Delta_{a,i} = \delta_c + \delta_{pc} = F_a\langle S_z \rangle_i + G_a B_0^2 D_i \quad (1)$$

Because the values of $\langle S_z \rangle_i$ and D_i are constants that have been calculated for each Ln^{3+} ion,[133−136] eq 1 can be rearranged into the two forms shown in eqs 2 and 3.[137,138]

$$\Delta_{a,i}/D_i = F_a\langle S_z \rangle_i/D_i + G_a B_0^2 \quad (2)$$

$$\Delta_{a,i}/\langle S_z \rangle_i = F_a + G_a B_0^2 D_i/\langle S_z \rangle_i \quad (3)$$

dx.doi.org/10.1021/ic201852j | Inorg. Chem. 2012, 51, 7050−7065

Table 8. Major Fragments Observed in the FI Mass Spectra of $Ln(H_3BNMe_2BH_3)_3$ Complexes

	ML_2^+		ML_3^+		$M_2L_5^+$		$M_3L_8^+$	
M	mass (m/z)	rel. int. (%)	mass (m/z)	rel. int. (%)	mass (m/z)	rel. int. (%)	mass (m/z)	rel. int. (%)
La (**2b**)	282	50	353	80	637	100	991	80
Ce (**3b**)	285	5	356	100	639	35	995	5
Pr (**4b**)	285	35	356	65	642	35	999	10
Nd (**5b**)	288	55	358	100	648	95	1007	10
Sm (**6b**)	296	95	367	80	660	100	1029	10
Gd (**8b**)	300	100	370	90	674	95	1042	10
Tb (**9b**)	303	40	373	65	677	100	1051	4
Dy (**10b**)			377	100	684	40		
Ho (**11b**)	309	90	379	80	688	100		
Y[a] (**1b**)	233	65	303	100	537	90		
Er (**12b**)			381	100	693	15		
Tm (**13b**)	312	45	383	100	700	85		
Lu (**15b**)	318	70	390	100	709	80		

[a]Yttrium placed in the series according to its ionic radius; L = $H_3BNMe_2BH_3^-$.

Typically, these equations are used to analyze LIS values for a certain reporter nucleus in a series of complexes with the same general chemical formula but with different lanthanide ions. In such cases, if plots of $\Delta_{a,i}/\langle S_z\rangle_i$ vs $D_i/\langle S_z\rangle_i$, or of $\Delta_{a,i}/D_i$ vs $\langle S_z\rangle_i/D_i$, for different lanthanide ions give points that fall on a straight line, then this implies that the geometric factor G_a (as well as the crystal field parameter B_0^2 and the contact shift factor F_a) is the same for all the complexes, and thus the complexes are very likely isostructural.[139]

The ^1H and ^{11}B NMR spectra of the paramagnetic lanthanide DMADB complexes exhibit resonances that are broadened and shifted to varying degrees depending on the identity of the lanthanide ion. For the thf free complexes, we measured three different sets of LIS data in deuterobenzene at room temperature: the ^{11}B shifts of the BH_3 groups, and the ^1H shifts of the BH_3 and NMe_2 groups. For the thf complexes, we also measured the ^1H shifts of the α and β thf resonances. The ^{11}B resonances could be observed as broadened singlets for all the complexes except that of Gd, for which no resonances could be seen owing to rapid relaxation of the ^{11}B nuclei by this highly paramagnetic ion. For similar reasons, ^1H NMR resonances for the BH_3 group could be observed for all complexes except Eu, Gd, Tb, Dy, Ho, and Er; also ^1H NMR resonances could be observed for the NMe_2 and α and β thf protons for all except Eu and Gd. Note that, for the base-free compounds, pure samples of the Eu and Yb complexes could not be prepared, but we were able to measure the ^{11}B NMR shift of $Eu(H_3BNMe_2BH_3)_3$ from a mixture that contained this species.

In all cases, only a single BH_3 resonance and a single NMe_2 resonance are present in the NMR spectra (the same is true for the α and β thf protons); thus, these complexes must be dynamic in solution. The effective (i.e., time averaged) symmetry of these complexes is at least axial, and very likely cubic, and thus the LIS shifts should be amenable to analysis by eqs 1−3. Structural differences across the series, if present, should be detectable, because the dynamic processes will average different ensembles of structures.

Table 9 shows an analysis of the ^1H and ^{11}B LIS data for the $Ln(H_3BNMe_2BH_3)_3$ and $Ln(H_3BNMe_2BH_3)_3(thf)$ complexes.[140] It has been previously pointed out that eq 2 is better suited when the contact term makes a larger contribution to the LIS than the pseudocontact term.[139] Owing to their close proximity to the lanthanide ions, the BH_3 groups experience large contact contributions (denoted by the values of F_a in Table 9), and fits of the ^1H and ^{11}B LIS data for the BH_3 groups to eq 2 are linear with high correlation coefficients (Figure 9). The contact contributions for the NMe_2 and thf resonances are much smaller owing to their larger distances from the metal center, with the contact contribution for the α

Table 9. ^1H and ^{11}B LIS Data for Lanthanide DMADB Complexes Using eqs 2 and 3

nucleus	eqn used	# metals	F_a	B_0^2	R^2
		$Ln(H_3BNMe_2BH_3)_3(thf)$			
BH_3 (^{11}B)	2	10	−21.9	−0.48	0.971
BH_3 (^1H)	2	5	−18.5	0.60	0.995
NMe_2 (^1H)	3	7 [a]	0.050	0.23	0.806
α-thf (^1H)	3	7 [a]	0.215	−0.66	0.798
β-thf (^1H)	3	7 [a]	−0.0205	−0.48	0.900
		$Ln(H_3BNMe_2BH_3)_3$			
BH_3 (^{11}B)	2	8 [b]	−21.4	−4.2	0.925
BH_3 (^1H)	2	3	−17.7	−1.08	0.999
NMe_2 (^1H)	3	7 [a]	1.03	−0.64	0.825

[a]The Tm and Yb data were omitted from the least-squares fit. [b]Excludes Eu data because the formation of $Eu(H_3BNMe_2BH_3)_3$ could not be verified by other analytical techniques.

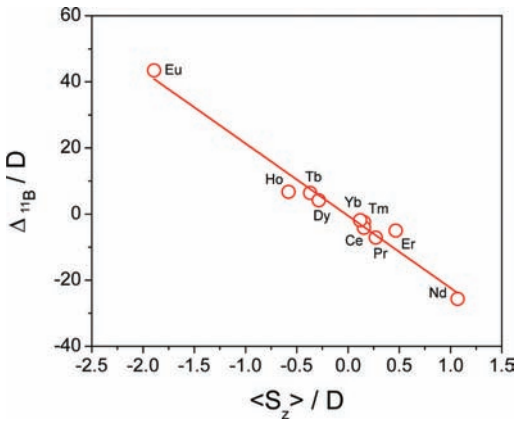

Figure 9. Plot of $\Delta_{a,i}/D$ vs $\langle S_z\rangle_i/D$ (eq 2) for the lanthanide induced shifts of the ^{11}B NMR resonances in the paramagnetic $Ln(H_3BNMe_2BH_3)_3(thf)$ complexes.

dx.doi.org/10.1021/ic201852j | Inorg. Chem. 2012, 51, 7050−7065

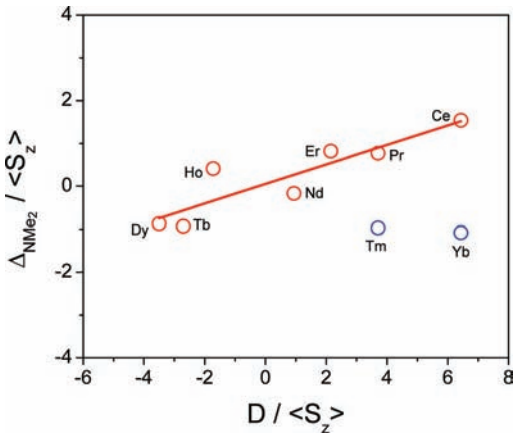

Figure 10. Plot of $\Delta_{a,i}/\langle S_z\rangle_i$ vs $D/\langle S_z\rangle_i$ (eq 3) for the lanthanide induced shifts of the ^{1}H NMR resonances of the NMe_2 groups in the paramagnetic $Ln(H_3BNMe_2BH_3)_3(thf)$ complexes. The least-squares fit excluded the points for Tm and Yb.

resonances of thf being larger than for the β resonances, as expected. Fits of these data to eq 3 are linear (Figure 10), but the points for Tm and Yb fall distinctly off the line generated by the other elements.

Although there is some scatter in all of the plots, the data are most consistent with the conclusion that, in benzene solution, all of the $Ln(H_3BNMe_2BH_3)_3$ complexes are isostructural with one another, as are the $Ln(H_3BNMe_2BH_3)_3$(thf) complexes, except for those with Ln = Tm or Yb (and also, by inference, Lu). For the base-free complexes, this finding is interesting because these compounds adopt a variety of solid state structures. If we assume that the complexes of Y, Dy, and Er, which are dinuclear in the solid state, dissolve with retention of the dinuclear structure, then the LIS data suggest that the polymeric $Ln(H_3BNMe_2BH_3)_3$ complexes readily break up in solution to their respective dimeric forms. This respeciation would also account for why the polymeric $Ln(H_3BNMe_2BH_3)_3$ complexes are soluble in hydrocarbon solvents.

To address residual doubts about whether the scatter in the plots was too large to conclude that the complexes are isostructural, and also to obtain additional evidence that the Tm and Yb complexes adopt different structures, we carried out an alternative analysis of the LIS data. It has been pointed out that low correlation coefficients for the least-squares fits to eqs 2 and 3 can result from a failure of any of the underlying assumptions. In this context, Reuben has noted that the crystal field parameter B_0^2 is not strictly invariant across the series of lanthanides.[141] In particular, it is quite common for the late lanthanides Yb and especially Tm to deviate from the least-squares lines obtained by fits to eqs 2 and 3,[142−146] and the deviations for Tm have been attributed in at least one case to the larger than expected value for B_0^2 relative to the other lanthanide ions.[147]

To factor out this effect, we employed a method to analyze the LIS data that is independent of B_0^2.[141] This method combines eq 1 for two different nuclei (designated by the indices a and b) within the same complex, eliminating the B_0^2 term, to give eq 4:

$$\Delta_{a,i}/\langle S_z\rangle_i = (F_a - R_{ab}F_b) + R_{ab}\Delta_{b,i}/\langle S_z\rangle_i \qquad (4)$$

If a series of lanthanide complexes is isostructural across the period, a plot of $\Delta_{a,i}/\langle S_z\rangle_i$ vs $\Delta_{b,i}/\langle S_z\rangle_i$ using eq 4 should be linear with a slope of R_{ab} ($R_{ab} = G_a/G_b$), and an intercept of $(F_a - R_{ab}F_b)$. Deviations from linearity in such a plot can be attributed to changes in the value of R_{ab} (i.e., a change in structure), provided that all other assumptions are valid (especially the assumption of axial symmetry).

For the $Ln(H_3BNMe_2BH_3)_3$(thf) complexes, plots of $\Delta_{a,i}/\langle S_z\rangle_i$ for the α and β thf resonances vs $\Delta_{b,i}/\langle S_z\rangle_i$ for the NMe_2 resonances result in highly linear trends for all the lanthanide ions except for Tm and Yb (Figure 11). This finding suggests

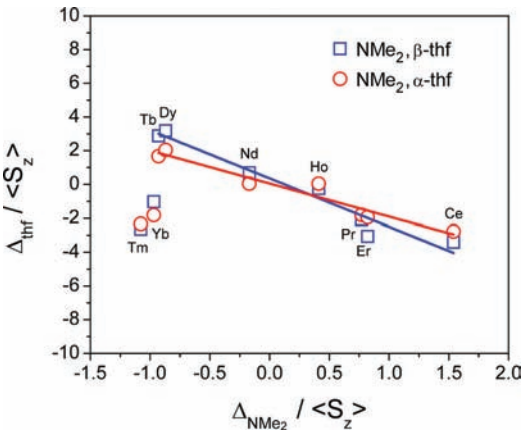

Figure 11. Plot of $\Delta_{a,i}/\langle S_z\rangle_i$ for the ^{1}H α (red) and β (blue) thf resonances vs $\Delta_{b,i}/\langle S_z\rangle_i$ for the NMe_2 resonances in the paramagnetic $Ln(H_3BNMe_2BH_3)_3$(thf) complexes. The least-squares fits excluded the points for Tm and Yb.

that the complexes of the latter two ions do indeed adopt a different structure. To corroborate the analysis, crystallographic studies of both the Tm and the Lu complexes were conducted, which confirmed that these two complexes adopt structures that are different from those of the earlier lanthanides. In particular, these two complexes are 12 coordinate instead of 13 coordinate because one Ln···B distance is longer than the rest (see above). The LIS analysis suggests that all of the $Ln(H_3BNMe_2BH_3)_3$(thf) complexes retain their solid state structures in hydrocarbon solutions.

Analysis of the base-free $Ln(H_3BNMe_2BH_3)_3$ complexes in terms of eq 4 is not possible because a second reporter nucleus (one without a large contact contribution) is not available.[141]

Thermogravimetric Analyses of $Ln(H_3BNMe_2BH_3)_3$(thf) and $Ln(H_3BNMe_2BH_3)_3$ Complexes. We have carried out thermogravimetric analyses (TGA) of the lanthanide aminodiboranate complexes to obtain quantitative assessments of their volatilities. The measurements were conducted under 0.3 Torr of N_2; under these conditions, sublimation occurs without significant decomposition and, for samarium through lutetium, at rates high enough to give good quantitative results.

For the thf adducts of stoichiometry $Ln(H_3BNMe_2BH_3)_3$(thf), the TGA traces show two features: a lower temperature feature due to loss of thf, and a higher temperature feature due to sublimation of the resulting base-free $Ln(H_3BNMe_2BH_3)_3$ material (Figure 12). The assignment of the higher temperature feature was confirmed from studies of isolated samples of the base-free materials, which give a single TGA peak at exactly the same temperature as the higher temperature peak seen for the thf adducts.

dx.doi.org/10.1021/ic201852j | Inorg. Chem. 2012, 51, 7050−7065

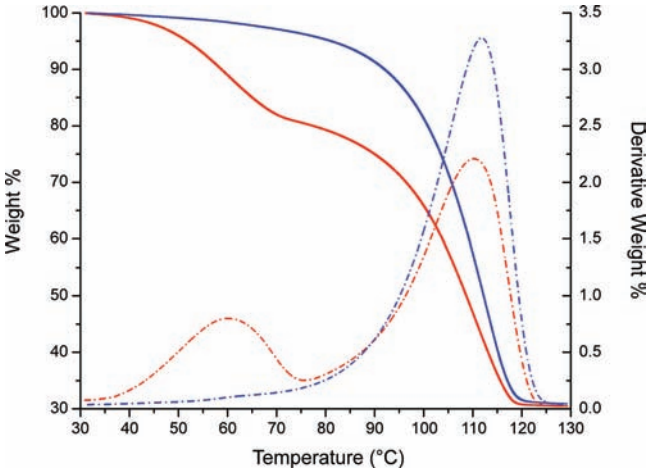

Figure 12. TGA traces (solid) with the corresponding first derivative plots (dashed) for $Tb(H_3BNMe_2BH_3)_3$(thf) (**9a**, red) and $Tb(H_3BNMe_2BH_3)_3$ (**9b**, blue), obtained at 1 °C/min at 0.3 Torr.

In most of the TGA studies, approximately 15−30% of nonvolatile residue remains after sublimation. As has been proposed in other systems,[57,59,61] it is likely that some (and perhaps most) of the nonvolatile material is generated by hydrolysis during the $T < 1$ min exposure to ambient humidity that occurs during loading of the sample into the instrument. During sample loading, crystals of the lanthanide complexes that are colored (i.e., Nd = purple, Er = pink, etc.) become noticeably lighter in color along the crystal edges. In separate larger scale studies, samples of the $Ln(H_3BNMe_2BH_3)_3$(thf) complexes that had not been exposed to air sublimed to afford the corresponding $Ln(H_3BNMe_2BH_3)_3$ complexes in isolated yields up to 96%.

The derivatives of the TGA traces reveal the temperatures at which the rate of weight change for each of these processes is at a maximum (Table 10). Comparison of these maxima reveals that the thf desolvation temperature decreases across the period from 78 °C (Sm) to 45 °C (Lu). Similarly, the sublimation temperature of the desolvated complex also decreases across the series. A representative set of TGA traces and first derivative plots is shown in Figure 12 (all taken at a temperature ramp of 1 °C/min). For example, the rate of thf loss from $Tb(H_3BNMe_2BH_3)_3$(thf), **9a**, peaks at 60.3 °C whereas the rate of sublimation peaks at about 112 °C. The latter temperature closely corresponds to the 110 °C temperature for the maximum sublimation rate of isolated samples of the base free material $Tb(H_3BNMe_2BH_3)_3$, **9b**.

Table 10. TGA Trace Data for Selected $Ln(H_3BNMe_2BH_3)_3$(thf) Complexes at 0.31 Torr and 1 °C/min and Comparison to Sublimation Yields Obtained without Atmospheric Exposure

	temp of max weight loss, T_{MWL} (°C)			
Ln	thf loss	sublimation	total wt loss (%)	subl yield (%) under inert conditions
Sm (**6a**)	78.1	121.3	>71	84
Gd (**8a**)	71.6	117.6	84	92
Tb (**9a**)	60.3	110.4	70	
Dy (**10a**)	61.9	112.4	82	
Ho (**11a**)	60.1	111.8	74	
Y[a] (**1a**)	61.1	106.7	80	
Er (**12a**)	53.6	104.8	72	96
Tm (**13a**)	48.8	105.1	68	91
Lu (**15a**)	48.5	103.8	76	96

[a]Yttrium has been placed in the series according to its ionic radius.

Isothermal TGA data collected from samples of the base-free complexes at 100 °C and 0.29 Torr of N_2 corroborate the observed trends in volatility (Figure 13). The mass decrease is initially linear with time, but slows at longer times because of depletion and surface area effects, as has been reported in other TGA sublimation studies.[57,61] Taking the initial rates of weight loss as a measure of volatility, a comparison of the isothermal data shows that there is a steady increase in sublimation rate across the lanthanide period from $Sm(H_3BNMe_2BH_3)_3$ at 0.25 mg/min to $Lu(H_3BNMe_2BH_3)_3$ at 1.23 mg/min (Table 11),

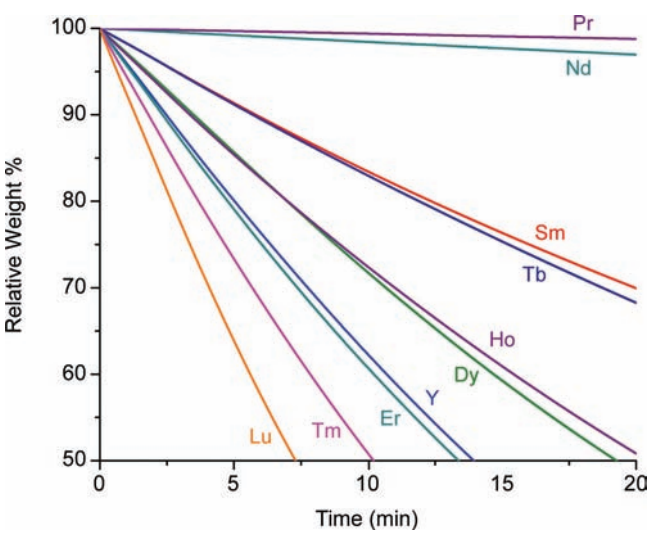

Figure 13. Isothermal TGA traces of selected $Ln(H_3BNMe_2BH_3)_3$ complexes obtained at 100 °C at 0.3 Torr.

Table 11. TGA Data for Selected $Ln(H_3BNMe_2BH_3)_3$ Complexes Collected at 0.29 Torr

	TGA trace at 1 °C/min		isothermal trace at 100 °C	
Ln	T_{MWL} (°C)	subl yield (%)	rate of subl[a] (mg/min)	subl yield (%)
Pr (**4b**)			0.01	
Nd (**5b**)			0.02	
Sm (**6b**)	115.9	73	0.25	70
Tb (**9b**)	111.7	69	0.33	73
Dy (**10b**)	109.6	81	0.51	80
Ho (**11b**)	109.7	72	0.51	78
Y[b] (**1b**)	107.8	91	0.70	90
Er (**12b**)	106.3	77	0.74	87
Tm (**13b**)	104.3	78	1.00	87
Lu (**15b**)	97.0	63	1.23	79

[a]Rate of sublimation measured to time required to reach 20% weight loss (t_{20}), for an initial charge of 15−20 mg. [b]Yttrium has been placed in the series according to its ionic radii.

for sample charges of 15−20 mg. The rates of sublimation for the earlier lanthanides $Pr(H_3BNMe_2BH_3)_3$ and $Nd(H_3BNMe_2BH_3)_3$ are slow under these conditions, 0.01 and

dx.doi.org/10.1021/ic201852j | Inorg. Chem. 2012, 51, 7050−7065

0.02 mg/min, respectively, and these TGA studes were stopped before sublimation was complete. Overall, the TGA data closely track the sublimation temperatures, which for the entire lanthanide series range from 65 to 125 °C at 10^{-2} Torr.

The $Ln(H_3BNMe_2BH_3)_3$ complexes appear to be some of the most volatile lanthanide compounds ever reported. The silylamide complexes $Ln[N(SiMe_3)_2]_3$ and certain functionalized β-ketoiminates are also appreciably volatile, but these complexes require pressures 2 orders of magnitude lower than the aminodiboranates to sublime at comparable temperatures. Among lanthanide β-diketonates, complexes of stoichiometry $Ln(thd)_3$ (thd = 2,2,6,6-tetramethyl-3,5-heptanedionate) are among the most volatile and are commonly used in CVD processes.[12] The thd derivatives have been used previously as a benchmark for volatility comparisons of lanthanide CVD precursors.[61] We made a direct comparison of the TGA traces of $Er(thd)_3$, and our erbium compound $Er(H_3BNMe_2BH_3)_3$, **12b**, under identical conditions (Supporting Information, Figure S2). The traces clearly show that the latter sublimes about 30 °C lower than $Er(thd)_3$ under identical conditions.

Interestingly, the $Ln(H_3BNMe_2BH_3)_3$ complexes are highly volatile, even for those that are polymeric in the solid state. Polymerization typically leads to lowered volatility owing to the increased energy required to free molecules from covalent bonding interactions (as opposed to weaker van der Waals interactions) with their neighbors, and to compensate for the reorganization energy required to induce the conformational change that attends the depolymerization process. It has been shown, however, that homoleptic tetrahydroborate complexes such as $U(BH_4)_4$, which also has a polymeric 14-coordinate solid-state structure but is highly volatile, has a low barrier to ligand-rearrangement to the volatile, 12-coordinate monomeric form.[148,149]

Consistent with the above considerations, the lowest sublimation rates are seen for the DMADB complexes of the earlier $Pr(H_3BNMe_2BH_3)_3$ (**4b**) and $Nd(H_3BNMe_2BH_3)_3$ (**5b**). The Pr compound (and probably Nd as well) adopts a polymeric structure with $Ln(\kappa^3\text{-}H_3BNMe_2BH_3\text{-}\kappa^3)Ln$ bridging ligands. Evidently, the volatilities of these 14-coordinate compounds are reduced owing to the reorganization energy required to convert them to a volatile (probably monomeric or dimeric) form. Intermediate volatilities are seen for the DMADB complexes of the midlanthanides $Sm(H_3BNMe_2BH_3)_3$ (**6b**) and $Tb(H_3BNMe_2BH_3)_3$ (**9b**). The Sm complex (and probably those of Eu, Gd, and Tb) adopts a weakly polymerized structure, in which tris(chelate) monomers are associated into chains by means of one intermolecular Ln−H-B interaction. Only this bond needs to be broken to convert the polymer into monomers. The highest volatilities are seen for the late lanthanides Dy through Lu (and including Y). All of these DMADB complexes adopt dinuclear structures with no strong interactions between the dimers in the solid state. These 12 coordinate complexes may sublime as dimers, or they may be able to rearrange into the corresponding $Ln(H_3BNMe_2BH_3)_3$ monomers.

The field ionization MS data for the $Ln(H_3BNMe_2BH_3)_3$ complexes lend support to these conclusions. The ion $Ln(H_3BNMe_2BH_3)_3^+$ and the dinuclear fragment $Ln_2(H_3BNMe_2BH_3)_5^+$ can be observed in the spectra of all of the complexes, and the trinuclear fragment $Ln_3(H_3BNMe_2BH_3)_8^+$ can be observed in the spectra of the larger lanthanides (Table 8). Care must be taken when drawing inferences from mass spectra because the ionization process can affect the chemistry, but the data support the hypothesis that the gas phase species responsible for sublimation of the $Ln(H_3BNMe_2BH_3)_3$ complexes are monomers and/or dimers for the late lanthanides, and possibly also trimers for the early lanthanides.

Solubility and Reactivity. The $Ln(H_3BNMe_2BH_3)_3(thf)$ complexes are soluble in nonpolar solvents such as pentane, benzene, toluene, and diethyl ether. They are also soluble in and unreactive toward dichloromethane, which is not the case for redox active DMADB complexes, such as $U(H_3BNMe_2BH_3)_3(thf)$.[104] The lanthanide complexes are slow to react with O_2 but react readily with water, the major hydrolysis products being lanthanide hydroxides, H_2, and (μ-dimethylamino)diborane, $(NMe_2)B_2H_5$.

The identity of the hydrolysis product $(NMe_2)B_2H_5$ has been established from the ^{11}B NMR spectrum of hydrolyzed lanthanide DMADB samples, which yields a triplet of doublets at about δ −17 in benzene.[150] The moisture-sensitivity is not surprising in view of the hydridic nature of the DMADB ligand and, as expected, these complexes are reactive toward most other protic reagents. The base-free complexes seem to be more susceptible to hydrolysis and are slightly less soluble in nonpolar solvents than their $Ln(H_3BNMe_2BH_3)_3(thf)$ counterparts.

We adventitiously obtained crystals of the partial hydrolysis product $[La(H_3BNMe_2BH_3)_2(OH)]_4$ (**16**), which presumably was generated by means of the following reaction:

$$Ln(H_3BNMe_2BH_3)_3(thf) + H_2O \rightarrow Ln(H_3BNMe_2BH_3)_2(OH) + H_2 + (NMe_2)B_2H_5$$

XRD studies of this material confirm that hydrolysis affords products bearing hydroxide ligands (Figure 14). The lanthanum

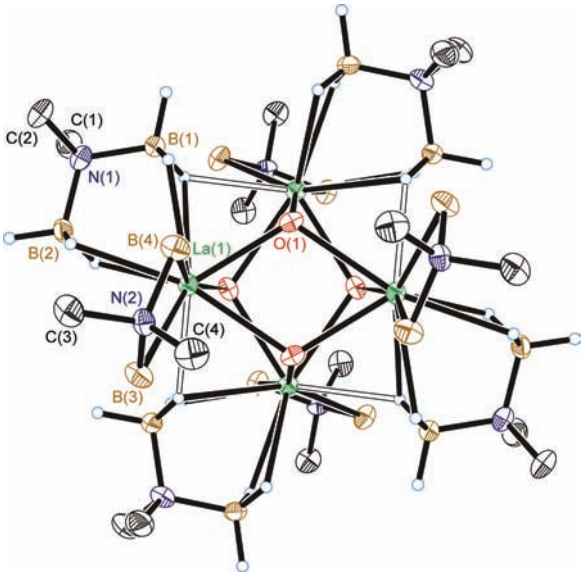

Figure 14. Molecular structure of $[La(H_3BNMe_2BH_3)_2(OH)]_4$, **16**. Ellipsoids are drawn at the 35% probability level, except for the hydrogen atoms, which are represented as arbitrarily sized spheres. Hydrogen atoms attached to all atoms except for B1 and B2 have been deleted for clarity. The interaction between the bridging B−H hydrogen atom on B1 and the adjacent La atom is depicted as an open bond for emphasis.

and oxygen atoms in **16** form the core of a distorted cube; each lanthanum atom is connected to three bridging hydroxyl groups and to two chelating DMADB ligands. One B−H bond of each

dx.doi.org/10.1021/ic201852j | Inorg. Chem. 2012, 51, 7050−7065

chelating DMADB ligand forms a bridge to an adjacent metal center; the La···B distances to the borane group that shares the hydride is considerably longer at 3.107(4) Å compared to 2.917(4)−2.982(4) Å distances for the other La···B contacts. The latter are similar to the average La···B distance of 2.94(2) Å observed in the thf adduct **2a**. The La−O bond distances of 2.443(2), 2.516(2), and 2.554(2) Å are similar to the Ln−O distance of 2.513(12) Å to the thf ligand in **2a**. These also compare well with other La−O bond distances reported for complexes containing a $La_3(\mu_3\text{-OH})$ core, which range from 2.417(2) to 2.583(12) Å.[69,151−153]

The hydrolysis of the $Ln(H_3BNMe_2BH_3)_3$ complexes, as detailed above, has important implications for the deposition of lanthanide oxides thin films. Carrying out depositions in the presence of water should readily convert the DMADB ligands into $(NMe_2)B_2H_5$, thereby providing a mechanism to form pure oxide films free of carbon, nitrogen, or boron heteratoms. The deposition of pure lanthanide oxide films by CVD from these DMADB complexes in the presence of water as a coreactant has already been demonstrated, as we have shown elsewhere.[109]

■ CONCLUDING REMARKS

We have described the synthesis and characterization of a new class of volatile lanthanide comounds: the tris(*N*,*N*-dimethylaminodiboranate) complexes and their thf adducts. For $Ln(H_3BNMe_2BH_3)_3(thf)$ in the solid state, the metal centers are 13-coordinate for the larger lanthanides Ln = La−Er, but are 12 coordinate for the smaller lanthanides Ln = Tm−Lu. The difference in structure also persists in solution, as shown by analysis of the lanthanide-induced NMR shifts. The structures of the base-free $Ln(H_3BNMe_2BH_3)_3$ complexes are polymeric, and the coordination numbers decrease from 14 (Ln = Pr) to 13 (Ln = Sm) to 12 (Ln = Dy, Y, Er) as the size of the lanthanide ion decreases. The $Ln(H_3BNMe_2BH_3)_3(thf)$ complexes lose thf when heated under vacuum before subliming as their respective base-free complexes. Despite their polymeric structures, the lanthanide *N*,*N*-dimethylaminodiboranates are highly volatile and have been shown to be effective CVD precursors for the deposition of lanthanide oxide films. Comprehensive details of CVD and ALD studies using $Ln(H_3BNMe_2BH_3)_3$ complexes will be forthcoming.

■ EXPERIMENTAL SECTION

All operations were carried out in vacuum or under argon using standard Schlenk techniques. All glassware was dried in an oven at 150 °C, assembled hot, and allowed to cool under vacuum before use. Tetrahydrofuran and pentane were distilled under nitrogen from sodium/benzophenone and degassed with argon immediately before use. Anhydrous $LnCl_3$ and LnI_3 were purchased from commercial vendors (Aldrich and Strem) and were used as received. $Na(H_3BNMe_2BH_3)$ was prepared by a literature route.[99]

Elemental analyses were carried out by the University of Illinois Microanalytical Laboratory. The IR spectra were recorded on a Nicolet Impact 410 infrared spectrometer as Nujol mulls between KBr plates. The ^{1}H NMR data were obtained on a Varian Unity 400 instrument at 400 MHz or on a Varian Unity U500 instrument at 500 MHz. The ^{11}B NMR data were collected on a General Electric GN300WB instrument at 96 MHz or on a Varian Unity Inova 600 instrument at 192 MHz. Chemical shifts are reported in δ units (positive shifts to high frequency) relative to TMS (^{1}H) or $BF_3{\cdot}Et_2O$ (^{11}B). Field ionization (FI) mass spectra were recorded on a Micromass 70-VSE mass spectrometer. The shapes of all peak envelopes correspond with those calculated from the natural abundance isotopic distributions in the observed spectra, except for the $Ln(H_3BNMe_2BH_3)_3^+$ and $Ln(H_3BNMe_2BH_3)_2(thf)^+$ fragments for the $Ln(H_3BNMe_2BH_3)_3(thf)$ complexes, which overlapped. Melting points and decomposition temperatures were determined in closed capillaries under argon on a Thomas-Hoover Unimelt apparatus. Thermogravimetric analysis (TGA) data were collected with a TA Instruments Q600 SDT simultaneous DSC-TGA instrument.

Representative Syntheses of $Ln(H_3BNMe_2BH_3)_3(thf)$ Complexes. *Tris(N,N-dimethylaminodiboranato)(tetrahydrofuran)-samarium(III), $Sm(H_3BNMe_2BH_3)_3(thf)$, (**6a**).* To a suspension of $SmCl_3$ (0.30 g, 1.2 mmol) in thf (20 mL) at 0 °C was added a solution of sodium *N*,*N*-dimethylaminodiboranate (0.33 g, 3.5 mmol) in thf (20 mL). The light yellow reaction mixture was stirred at 0 °C for 15 min before being allowed to warm to room temperature. The resulting mixture was stirred for 15 h and then evaporated to dryness under vacuum to afford a sticky, ivory-colored solid. The residue was extracted with pentane (2 × 15 mL), and the extracts were combined, filtered, concentrated to about 15 mL, and cooled to −20 °C to yield 0.18 g of large, ivory-colored crystals. The mother liquor was concentrated to 7 mL and cooled to −20 °C to yield an additional 0.11 g of ivory-colored crystals. Yield: 0.29 g (57%). M.p.: 134−135 °C. Anal. Calcd for $C_{10}H_{44}B_6N_3OSm$: C, 27.4; H, 10.1; N, 9.60. Found: C, 27.6; H, 10.5; N, 9.73. ^{1}H NMR (C_6D_6, 20 °C): δ −1.86 (br 1:1:1:1 q, J_{BH} = 104 Hz, BH_3, 18H), 1.29 (s, fwhm = 10 Hz, β-CH_2, 4H), 3.80 (s, fwhm = 14 Hz, OCH_2, 4H), 2.25 (s, fwhm = 4 Hz, NMe_2, 18H). ^{11}B NMR (C_6D_6, 20 °C): δ −9.8 (br q, J_{BH} = 87 Hz, BH_3). MS(FI) [fragment ion, relative abundance]: *m*/*z* 239 $[Sm(H_3BNMe_2BH_3)(BH_4)^+$, 20], 296 $[Sm(H_3BNMe_2BH_3)_2^+$, 60], 362 $[Sm(H_3BNMe_2BH_3)_3^+/Sm(H_3BNMe_2BH_3)_2(thf)^+$, 100], 660 $[Sm_2(H_3BNMe_2BH_3)_5^+$, 80], 732 $[Sm_2(H_3BNMe_2BH_3)_5(thf)^+$, 5]. IR (cm^{-1}): 2496 sh, 2392 vs, 2344 m, 2286 s, 2255 m, 2218 vs, 2173 s, 2067 w, 1268 s, 1238 s, 1216 s, 1187 m, 1170 s, 1137 s, 1114 sh, 1034 sh, 1019 s, 962 w, 924 m, 902 w, 856 m, 838 w, 814 w, 723 w, 667 w, 457 m.

*Tris(N,N-dimethylaminodiboranato)(tetrahydrofuran)cerium(III), $Ce(H_3BNMe_2BH_3)_3(thf)$, (**3a**).* To a suspension of CeI_3 (0.95 g, 1.8 mmol) in thf (20 mL) at 0 °C was added a solution of sodium *N*,*N*-dimethylaminodiboranate (0.52 g, 5.5 mmol) in thf (20 mL). The white reaction mixture was stirred at 0 °C for 15 min before being allowed to warm to room temperature. The resulting mixture was stirred for 15 h and then evaporated to dryness under vacuum to afford a sticky, white solid. The residue was extracted with pentane (65 mL), the extract was filtered, and the clear filtrate was concentrated to about 18 mL and cooled to −20 °C to yield 0.49 g of large, colorless blocks. The mother liquor was concentrated to 6 mL and cooled to −20 °C to yield an additional 0.085 g of crystals. Yield: 0.58 g (74%). M.p.: 132−134 °C. Anal. Calcd for $C_{10}H_{44}B_6N_3OCe$: C, 28.1; H, 10.4; N, 9.83. Found: C, 27.9; H, 10.8; N, 9.65. ^{1}H NMR (C_6D_6, 20 °C): δ 0.79 (s, fwhm = 6 Hz, NMe_2, 18H), 3.84 (s, fwhm = 12 Hz, β-CH_2, 4H), 7.11 (s, fwhm = 22 Hz, OCH_2, 4H), 20.39 (br 1:1:1:1 q, J_{BH} = 92 Hz, BH_3, 18H). ^{11}B NMR (C_6D_6, 20 °C): δ 23.1 (br s, fwhm = 49 Hz, BH_3). MS(FI) [fragment ion, relative abundance]: *m*/*z* 72 [thf, 100], 355 $[Ce(H_3BNMe_2BH_3)_3^+/Ce(H_3BNMe_2BH_3)_2(thf)^+$, 15], 414 $[Ce(H_3BNMe_2BH_3)_3(thf)^+$, 2], 640 $[Ce_2(H_3BNMe_2BH_3)_5^+$, 5], 710 $[Ce_2(H_3BNMe_2BH_3)_5(thf)^+$, 2]. IR (cm^{-1}): 2492 sh, 2390 s, 2340 w, 2285 m, 2255 sh, 2216 vs, 2168 sh, 2064 w, 1261 s, 1235 s, 1216 s, 1186 s, 1169 vs, 1138 s, 1032 sh, 1017 s, 929 w, 901 w, 855 m, 836 w, 809 w, 722 w, 666 w, 449 m.

*Tris(N,N-dimethylaminodiboranato)(tetrahydrofuran)-lanthanum(III), $La(H_3BNMe_2BH_3)_3(thf)$, (**2a**).* To $La(H_3BNMe_2BH_3)_3$ (0.10 g, 0.28 mmol) was added 15 mL of thf. The resulting clear solution was stirred for 15 min and evaporated to dryness under vacuum. The white residue was extracted with pentane (40 mL), the extract was filtered, and the clear filtrate was concentrated to 10 mL and stored at −20 °C to yield large, cubic crystals. Yield: 0.06 g (50%). M.p.: 136−137 °C. Anal. Calcd for $C_{10}H_{44}B_6N_3OLa$: C, 28.2; H, 10.4; N, 9.86. Found: C, 27.9; H, 11.0; N, 9.65. ^{1}H NMR (C_6D_6, 20 °C): δ 1.13 (m, β-CH_2, 4H), 2.30 (s, NMe_2, 18H), 2.87 (br 1:1:1:1 q, J_{BH} = 82 Hz, BH_3, 18H), 3.78 (m, OCH_2, 4H). ^{11}B NMR (C_6D_6, 20 °C): δ −2.87 (br q, J_{BH} = 91 Hz, BH_3). MS(FI) [fragment ion, relative abundance]: *m*/*z* 114 $[(H_2BNMe_2)_2$, 100], 226 $[La(H_3BNMe_2BH_3)$-

dx.doi.org/10.1021/ic201852j | Inorg. Chem. 2012, 51, 7050−7065

$(BH_4)^+$, 10], 283 [$La(H_3BNMe_2BH_3)_2^+$, 25], 353 [$La(H_3BNMe_2BH_3)_3^+$/$La(H_3BNMe_2BH_3)_2(thf)^+$, 100], 636 [$La_2(H_3BNMe_2BH_3)_5^+$, 30]. IR ($cm^{-1}$): 2487 sh, 2421 sh, 2390 s, 2339 m, 2288 m, 2259 sh, 2220 vs, 2181 sh, 2064 w, 1399 w, 1259 s, 1236 s, 1218 s, 1188 m, 1170 vs, 1141 s, 1034 sh, 1017 s, 930 m, 901 w, 855 w, 836 w, 808 w, 723 w, 667 w, 445 m.

Representative Syntheses of $Ln(H_3BNMe_2BH_3)_3$ Complexes. *Tris(N,N-dimethylaminodiboranato)terbium(III), $Tb(H_3BNMe_2BH_3)_3$, (**9b**).* $TbCl_3$ (0.46 g, 1.7 mmol) and sodium *N,N*-dimethylaminodiboranate (0.49 g, 5.2 mmol) were added to a 100 mL round-bottom Schlenk flask with 30−40 steel balls (4.5-mm diameter). The flask was gently agitated by hand for 25 min. Sublimation at 90−100 °C and 10^{-2} Torr afforded white crystals. Yield: 0.23 g (36%). M.p.: 159 °C (dec). Anal. Calcd for $C_6H_{36}N_3B_6Tb$: C, 19.3; H, 10.1; N, 11.2. Found: C, 19.6; H, 10.1; N, 11.2. ^1H NMR (C_6D_6, 20 °C): δ 118.8 (s, fwhm = 3300 Hz, NMe_2). ^{11}B NMR (C_6D_6, 20 °C): δ −343.8 (s, fwhm = 690 Hz, BH_3). MS (FI): *m/z* 246 [$Tb(H_3BNMe_2BH_3)(BH_4)^+$, 2], 303 [$Tb(H_3BNMe_2BH_3)_2^+$, 40], 373 [$Tb(H_3BNMe_2BH_3)_3^+$, 65], 620 [$Tb_2(H_3BNMe_2BH_3)_4(BH_4)^+$, 5], 677 [$Tb_2(H_3BNMe_2BH_3)_5^+$, 100], 1051 [$Tb_3(H_3BNMe_2BH_3)_8^+$, 4]. IR ($cm^{-1}$): 2420 vs, 2336 m, 2270 m, 2217 vs, 2169 s, 2129 sh, 2059 w, 1400 w, 1327 w, 1281 s, 1239 m, 1218 m, 1184 m, 1166 m, 1158 s, 1132 m, 1032 w, 1018 s, 975 w, 928 m, 904 w, 844 w, 815 w, 726 w, 459 m.

*Tris(N,N-dimethylaminodiboranato)lutetium(III), $Lu(H_3BNMe_2BH_3)_3$, (**14b**).* Sublimation of **14a** (0.32 g, 0.69 mmol) at 65−75 °C and 10^{-2} Torr afforded white microcrystals. Yield: 0.26 g (96%). M.p.: 147 °C (dec). Anal. Calcd for $C_6H_{36}B_6N_3Lu$: C, 18.5; H, 9.30; N, 10.8. Found: C, 18.2; H, 9.74; N, 10.4. ^1H NMR (C_6D_6, 20 °C): δ 2.10 (s, fwhm = 4 Hz, NMe_2), 3.19 (br 1:1:1:1 q, J_{BH} = 87 Hz, BH_3). ^{11}B NMR (C_6D_6, 20 °C): δ −6.27 (q, J_{BH} = 90 Hz, BH_3). MS(FI) [fragment ion, relative abundance]: *m/z* 261 [$Lu(H_3BNMe_2BH_3)(BH_4)^+$, 5], 318 [$Lu(H_3BNMe_2BH_3)_2^+$, 70], 377 [$Lu(H_3BNMe_2BH_3)_3^+-BH_2$, 15], 390 [$Lu(H_3BNMe_2BH_3)_3^+$, 100], 709 [$Lu_2(H_3BNMe_2BH_3)_5^+$, 80]. IR ($cm^{-1}$): 2424 vs, 2341 m, 2274 m, 2228 vs, 2173 s, 2142 sh, 2060 w, 1433 w, 1401 w, 1342 w, 1298 s, 1241 m, 1220 m, 1188 m, 1164 s, 1143 m, 1133 m, 1032 sh, 1020 s, 972 w, 928 m, 907 w, 842 w, 820 w, 724 w, 472 m.

Crystallographic Studies.[154] Single crystals of **1a**, **2a**, **10a**, **1b**, **4b**, **6b**, **10b**, and **12b**, grown by sublimation, were mounted on glass fibers with Paratone-N oil (Exxon) or Krytox oil (Dupont) and immediately cooled to −80 °C in a cold nitrogen gas stream on the diffractometer. Single crystals of **5a**−**8a**, **12a**, and **16** were crystallized from pentane and treated similarly. Standard peak search and indexing procedures, followed by least-squares refinement, yielded the cell dimensions given in the Supporting Information, Tables S1−S3. Data were collected with an area detector by using the measurement parameters listed in the Supporting Information, Tables S1−S3. For all crystals, the measured intensities were reduced to structure factor amplitudes, and their estimated standard deviations by correction for background and Lorentz and polarization effects. Although corrections for crystal decay were unnecessary, face-indexed absorption corrections were applied. Systematically absent reflections were deleted, and symmetry equivalent reflections were averaged to yield the set of unique data. Unless specified otherwise, all unique data were used in the least-squares refinement.

The structures were solved using direct methods (SHELXTL). The correct position of all the non-hydrogen atoms were deduced from *E*-maps and subsequent difference Fourier calculations. The analytical approximations to the scattering factors were used, and all structure factors were corrected for both real and imaginary components of anomalous dispersion. Unless otherwise stated, the refinement models had the following features: (1) Independent anisotropic displacement factors were refined for the non-hydrogen atoms. (2) Hydrogen atoms were placed in idealized positions with C−H = 0.99 and 0.98 Å for methylene and methyl hydrogen atoms, respectively, and with B−H = 1.15 Å for the boranyl hydrogen atoms. (3) The methyl and boranyl groups were allowed to rotate about the C−N and B−N bonds to find the best least-squares positions. (4) Methyl hydrogen atoms were given displacement parameters equal to 1.5 times U_{eq} for the attached carbon atom, whereas for the boranyl hydrogen atoms and methylene hydrogen atoms the multiplier was 1.2. For all data sets, successful convergence was indicated by the maximum shift/error of <0.002 for the last cycle. Unless otherwise stated, a final analysis of variance between observed and calculated structure factors showed no apparent errors. Final refinement parameters and characteristics specific to the individual refinements are given in the Supporting Information.

■ ASSOCIATED CONTENT

Ⓢ Supporting Information

Full experimental details and X-ray crystallographic data (CIF format). This material is available free of charge via the Internet at http://pubs.acs.org.

■ AUTHOR INFORMATION

Corresponding Author

*E-mail: ggirolam@illinois.edu.

■ ACKNOWLEDGMENTS

We thank the National Science Foundation (CHE11-12360) and the PG Research Foundation for support of this research, and Scott Wilson, Teresa Wieckowska-Prussak, and Danielle Gray for collecting the XRD data.

■ REFERENCES

(1) MacManus-Driscoll, J. L. *Adv. Mater.* **1997**, *9*, 457−473.
(2) Etourneau, J. *J. Less-Common Met.* **1985**, *110*, 267−281.
(3) Broers, A. N. *Rev. Sci. Instrum.* **1969**, *40*, 1040−1045.
(4) Mumaw, V. R.; Munger, B. L. In *Proceedings of the 35th Annual Meeting of the Electron Microscopy Society of America*; 1977; Vol. 35, pp 64−65.
(5) Joy, D. C.; Schmidt, P. H. Low work function hexaboride electron source. U.S. Patent 4,200,555, April 29, 1980.
(6) Gasgnier, M. *J. Mater. Sci.* **1991**, *26*, 1989−1999.
(7) Collocott, S. J.; Dunlop, J. B.; Lovatt, H. C.; Ramsden, V. S. *Mater. Sci. Forum* **1999**, *315*−*317*, 77−83.
(8) Buenzli, J.-C. G.; Piguet, C. *Chem. Soc. Rev.* **2005**, *34*, 1048−1077.
(9) Monocorgé, R. *Springer Ser. Mater. Sci.* **2005**, *83*, 320−378.
(10) Srivastava, A. M. *Uses of phosphors in display technologies. Handbook of Luminescence, Display Materials, and Devices*; Nalwa, H. S., Rohwer, L. S., Eds.; American Scientific Publishers: Los Angeles, CA, 2003; Vol. 3, pp 79−100.
(11) Haerkoenen, G.; Leppaenen, M.; Soininen, E.; Toernqvist, R.; Viljanen, J. *J. Alloys Compd.* **1995**, *225*, 552−554.
(12) Tiitta, M.; Niinistö, L. *Chem. Vap. Deposition* **1997**, *3*, 167−182.
(13) Leskelä, M. *J. Alloys Compd.* **1998**, *275*−*277*, 702−708.
(14) Bénalloul, P.; Barthou, C.; Benoit, J. *J. Alloys Compd.* **1998**, *275*−*277*, 709−714.
(15) Tanabe, S. *C. R. Chim.* **2002**, *5*, 815−824.
(16) Kido, J.; Okamoto, Y. *Chem. Rev.* **2002**, *102*, 2357−2368.
(17) de Bettencourt-Dias, A. *Dalton Trans.* **2007**, 2229−2241.
(18) Escribano, P.; Julian-Lopez, B.; Planelles-Arago, J.; Cordoncillo, E.; Viana, B.; Sanchez, C. *J. Mater. Chem.* **2008**, *18*, 23−40.
(19) Carlos, L. D.; Ferreira, R. A. S.; de Zea Bermudez, V.; Ribeiro, S. J. L. *Adv. Mater.* **2009**, *21*, 509−534.
(20) Binnemans, K. *Chem. Rev.* **2009**, *109*, 4283−4374.
(21) Scullin, M. L.; Yu, C.; Huijben, M.; Mukerjee, S.; Seidel, J.; Zhan, Q.; Moore, J.; Majumdar, A.; Ramesh, R. *Appl. Phys. Lett.* **2008**, *92*, 202113/1−202113/3.
(22) The International Technology Roadmap for Semiconductors. http://public.itrs.net/, 2010.

(23) Leskelä, M.; Kukli, K.; Ritala, M. *J. Alloys Compd.* **2006**, *418*, 27−34.
(24) Wilk, G. D.; Wallace, R. M.; Anthony, J. M. *J. Appl. Phys.* **2001**, *89*, 5243−5275.
(25) Wallace, R. M.; Wilk, G. *Mat. Res. Soc. Bull.* **2002**, *27*, 192−197.
(26) Robertson, J. *Eur. Phys. J.: Appl. Phys.* **2004**, *28*, 265−291.
(27) Locquet, J.-P.; Marchiori, C.; Sousa, M.; Fompeyrine, J.; Seo, J. W. *J. Appl. Phys.* **2006**, *100*, 051610/1−051610/14.
(28) Jones, A. C.; Aspinall, H. C.; Chalker, P. R.; Potter, R. J.; Kukli, K.; Rahtu, A.; Ritala, M.; Leskelä, M. *Mater. Sci. Eng., B* **2005**, *B118*, 97−104.
(29) Yanguas-Gil, A.; Yang, Y.; Kumar, N.; Abelson, J. R. *J. Vac. Sci. Technol., A* **2009**, *27*, 1235−1243.
(30) George, S. M. *Chem. Rev.* **2010**, *110*, 111−131.
(31) Aspinall, H. C. *Top. Appl. Phys.* **2007**, *106*, 53−72.
(32) Bradley, D. C.; Ghotra, J. S.; Hart, F. A. *J. Chem. Soc., Dalton Trans.* **1973**, 1021−1023.
(33) Kukli, K.; Ritala, M.; Pilvi, T.; Sajavaara, T.; Leskelä, M.; Jones, A. C.; Aspinall, H. C.; Gilmer, D. C.; Tobin, P. J. *Chem. Mater.* **2004**, *16*, 5162−5168.
(34) Triyoso, D. H.; Hegde, R. I.; Grant, J. M.; Schaeffer, J. K.; Roan, D.; White, B. E. Jr.; Tobin, P. J. *J. Vac. Sci. Technol., B* **2005**, *23*, 288−297.
(35) Kukli, K.; Ritala, M.; Pore, V.; Leskelä, M.; Sajavaara, T.; Hegde, R. I.; Gilmer, D. C.; Tobin, P. J.; Jones, A. C.; Aspinall, H. C. *Chem. Vap. Deposition* **2006**, *12*, 158−164.
(36) Scarel, G.; Wiemer, C.; Tallarida, G.; Spiga, S.; Seguini, G.; Bonera, E.; Fanciulli, M.; Lebedinskii, Y.; Zenkevich, A.; Pavia, G.; Fedushkin, I. L.; Fukin, G. K.; Domrachev, G. A. *J. Electrochem. Soc.* **2006**, *153*, F271−F276.
(37) Leskelä, M.; Niinistö, L.; Nykanen, E.; Soininen, P.; Tiitta, M. *Thermochim. Acta* **1991**, *175*, 91−98.
(38) Putkonen, M.; Sajavaara, T.; Johansson, L.-S.; Nunistö, L. *Chem. Vap. Deposition* **2001**, *7*, 44−50.
(39) Päiväsaari, J.; Putkonen, M.; Sajavaara, T.; Niinistö, L. *J. Alloys Compd.* **2004**, *374*, 124−128.
(40) Niinistö, J.; Petrova, N.; Putkonen, M.; Niinistö, L.; Arstila, K.; Sajavaara, T. *J. Cryst. Growth* **2005**, *285*, 191−200.
(41) Päiväsaari, J.; Putkonen, M.; Niinistö, L. *Thin Solid Films* **2005**, *472*, 275−281.
(42) Frohlich, K.; Luptak, R.; Dobrocka, E.; Husekova, K.; Cico, K.; Rosova, A.; Lukosius, M.; Abrutis, A.; Pisecny, P.; Espinos, J. P. *Mater. Sci. Semicond. Process.* **2007**, *9*, 1065−1072.
(43) Myllymäki, P.; Roeckerath, M.; Lopes, J. M.; Schubert, J.; Mizohata, K.; Putkonen, M.; Niinistö, L. *J. Mater. Chem.* **2010**, *20*, 4207−4212.
(44) Roeckerath, M.; Heeg, T.; Lopes, J. M. J.; Schubert, J.; Mantl, S.; Besmehn, A.; Myllymäki, P.; Niinistö, L. *Thin Solid Films* **2008**, *517*, 201−203.
(45) Wilkinson, G.; Birmingham, J. M. *J. Am. Chem. Soc.* **1954**, *76*, 6210.
(46) Birmingham, J. M.; Wilkinson, G. *J. Am. Chem. Soc.* **1956**, *78*, 42−44.
(47) Niinistö, J.; Putkonen, M.; Niinistö, L. *Chem. Mater.* **2004**, *16*, 2953−2958.
(48) Scarel, G.; Bonera, E.; Wiemer, C.; Tallarida, G.; Spiga, S.; Fanciulli, M.; Fedushkin, I. L.; Schumann, H.; Lebedinskii, Y.; Zenkevich, A. *Appl. Phys. Lett.* **2004**, *85*, 630−632.
(49) Malvestuto, M.; Scarel, G.; Wiemer, C.; Fanciulli, M.; D'Acapito, F.; Boscherini, F. *Nucl. Instrum. Methods Phys. Res., Sect. B* **2006**, *246*, 90−95.
(50) Losurdo, M.; Giangregorio, M. M.; Bruno, G.; Yang, D.; Irene, E. A.; Suvorova, A. A.; Saunders, M. *Appl. Phys. Lett.* **2007**, *91*, 091914/1−091914/3.
(51) Nolan, M.; Elliott, S. D. *Chem. Mater.* **2010**, *22*, 117−129.
(52) Lim, B. S.; Rahtu, A.; de Rouffignac, P.; Gordon, R. G. *Appl. Phys. Lett.* **2004**, *84*, 3957−3959.
(53) Päiväsaari, J.; Dezelah, C. L. I. V.; Back, D.; El-Kaderi, H. M.; Heeg, M. J.; Putkonen, M.; Niinistö, L.; Winter, C. H. *J. Mater. Chem.* **2005**, *15*, 4224−4233.
(54) Kwon, J.; Dai, M.; Halls, M. D.; Langereis, E.; Chabal, Y. J.; Gordon, R. G. *J. Phys. Chem. C* **2008**, *113*, 654−660.
(55) Bochkarev, M. N.; Maleev, A. A.; Balashova, T. V.; Fukin, G. K.; Baranov, E. V.; Efimova, Y. A.; Petrov, B. I.; Ilichev, V. A. *Inorg. Chim. Acta* **2008**, *361*, 2533−2539.
(56) Edelmann, F. T. *Chem. Soc. Rev.* **2009**, *38*, 2253−2268.
(57) Milanov, A. P.; Fischer, R. A.; Devi, A. *Inorg. Chem.* **2008**, *47*, 11405−11416.
(58) Milanov, A. P.; Thiede, T. B.; Devi, A.; Fischer, R. A. *J. Am. Chem. Soc.* **2009**, *131*, 17062−17063.
(59) Milanov, A. P.; Toader, T.; Parala, H.; Barreca, D.; Gasparotto, A.; Bock, C.; Becker, H.-W.; Ngwashi, D. K.; Cross, R.; Paul, S.; Kunze, U.; Fischer, R. A.; Devi, A. *Chem. Mater.* **2009**, *21*, 5443−5455.
(60) Belot, J. A.; Wang, A.; McNeely, R. J.; Liable-Sands, L.; Rheingold, A. L.; Marks, T. J. *Chem. Vap. Deposition* **1999**, *5*, 65−69.
(61) Edleman, N. L.; Wang, A.; Belot, J. A.; Metz, A. W.; Babcock, J. R.; Kawaoka, A. M.; Ni, J.; Metz, M. V.; Flaschenriem, C. J.; Stern, C. L.; Liable-Sands, L. M.; Rheingold, A. L.; Markworth, P. R.; Chang, R. P. H.; Chudzik, M. P.; Kannewurf, C. R.; Marks, T. J. *Inorg. Chem.* **2002**, *41*, 5005−5023.
(62) Herrmann, W. A.; Anwander, R.; Denk, M. *Chem. Ber.* **1992**, *125*, 2399−2405.
(63) Aspinall, H. C.; Gaskell, J.; Williams, P. A.; Jones, A. C.; Chalker, P. R.; Marshall, P. A.; Bickley, J. F.; Smith, L. M.; Critchlow, G. W. *Chem. Vap. Deposition* **2003**, *9*, 235−238.
(64) Aspinall, H. C.; Gaskell, J.; Williams, P. A.; Jones, A. C.; Chalker, P. R.; Marshall, P. A.; Smith, L. M.; Critchlow, G. W. *Chem. Vap. Deposition* **2004**, *10*, 13−17.
(65) Aspinall, H. C.; Gaskell, J.; Williams, P. A.; Jones, A. C.; Chalker, P. R.; Marshall, P. A.; Smith, L. M.; Critchlow, G. W. *Chem. Vap. Deposition* **2004**, *10*, 83−89.
(66) Aspinall, H. C.; Gaskell, J. M.; Loo, Y. F.; Jones, A. C.; Chalker, P. R.; Potter, R. J.; Smith, L. M.; Critchlow, G. W. *Chem. Vap. Deposition* **2004**, *10*, 301−305.
(67) Loo, Y. F.; Potter, R. J.; Jones, A. C.; Aspinall, H. C.; Gaskell, J. M.; Chalker, P. R.; Smith, L. M.; Critchlow, G. W. *Chem. Vap. Deposition* **2004**, *10*, 306−310.
(68) Potter, R. J.; Chalker, P. R.; Manning, T. D.; Aspinall, H. C.; Loo, Y. F.; Jones, A. C.; Smith, L. M.; Critchlow, G. W.; Schumacher, M. *Chem. Vap. Deposition* **2005**, *11*, 159−169.
(69) Aspinall, H. C.; Bickley, J. F.; Gaskell, J. M.; Jones, A. C.; Labat, G.; Chalker, P. R.; Williams, P. A. *Inorg. Chem.* **2007**, *46*, 5852−5860.
(70) Niinistö, L.; Päiväsaari, J.; Niinistö, J.; Putkonen, M.; Nieminen, M. *Phys. Status Solidi A* **2004**, *201*, 1443−1452.
(71) Deacon, G. B.; MacKinnon, P.; Dickson, R. S.; Pain, G. N.; West, B. O. *Appl. Organomet. Chem.* **1990**, *4*, 439−449.
(72) Gun'ko, Y. K.; Edelmann, F. T. *Comments Inorg. Chem.* **1997**, *19*, 153−184.
(73) Jones, A. C.; Aspinall, H. C.; Chalker, P. R.; Potter, R. J.; Kukli, K.; Rahtu, A.; Ritala, M.; Leskelä, M. *J. Mater. Chem.* **2004**, *14*, 3101−3112.
(74) Jones, A. C.; Aspinall, H. C.; Chalker, P. R.; Potter, R. J.; Manning, T. D.; Loo, Y. F.; O'Kane, R.; Gaskell, J. M.; Smith, L. M. *Chem. Vap. Deposition* **2006**, *12*, 83−98.
(75) Lo Nigro, R.; Malandrino, G.; Toro, R. G.; Fragalà, I. L. *Chem. Vap. Deposition* **2006**, *12*, 109−124.
(76) Malandrino, G.; Fragalà, I. L. *Coord. Chem. Rev.* **2006**, *250*, 1605−1620.
(77) Päiväsaari, J.; Niinistö, J.; Myllymäki, P.; Dezelah, C. I. V.; Winter, C. H.; Putkonen, M.; Nieminen, M.; Niinistö, L. *Top. Appl. Phys.* **2007**, *106*, 15−32.
(78) Jensen, J. A.; Gozum, J. E.; Pollina, D. M.; Girolami, G. S. *J. Am. Chem. Soc.* **1988**, *110*, 1643−1644.
(79) Kumar, N.; Yang, Y.; Noh, W.; Girolami, G. S.; Abelson, J. R. *Chem. Mater.* **2007**, *19*, 3802−3807.

(80) Kumar, N.; Yanguas-Gil, A.; Daly, S. R.; Girolami, G. S.; Abelson, J. R. *J. Am. Chem. Soc.* **2008**, *130*, 17660−17661.
(81) Sung, J.; Goedde, D. M.; Girolami, G. S.; Abelson, J. R. *J. Appl. Phys.* **2002**, *91*, 3904−3911.
(82) Jayaraman, S.; Yang, Y.; Kim, D. Y.; Girolami, G. S.; Abelson, J. R. *J. Vac. Sci. Technol., A* **2005**, *23*, 1619−1625.
(83) Jayaraman, S.; Gerbi, J. E.; Yang, Y.; Kim, D. Y.; Chatterjee, A.; Bellon, P.; Girolami, G. S.; Chevalier, J. P.; Abelson, J. R. *Surf. Coat. Technol.* **2006**, *200*, 6629−6633.
(84) Yang, Y.; Jayaraman, S.; Kim, D. Y.; Girolami, G. S.; Abelson, J. R. *Chem. Mater.* **2006**, *18*, 5088−5096.
(85) Yang, Y.; Jayaraman, S.; Kim, D. Y.; Girolami, G. S.; Abelson, J. R. *J. Cryst. Growth* **2006**, *294*, 389−395.
(86) Yang, Y.; Jayaraman, S.; Sperling, B.; Kim, D. Y.; Girolami, G. S.; Abelson, J. R. *J. Vac. Sci. Technol., A* **2007**, *25*, 200−206.
(87) Goedde, D. M.; Girolami, G. S. *J. Am. Chem. Soc.* **2004**, *126*, 12230−12231.
(88) Jayaraman, S.; Klein, E. J.; Yang, Y.; Kim, D. Y.; Girolami, G. S.; Abelson, J. R. *J. Vac. Sci. Technol., A* **2005**, *23*, 631−633.
(89) Goedde, D. M.; Windler, G. K.; Girolami, G. S. *Inorg. Chem.* **2007**, *46*, 2814−2823.
(90) Makhaev, V. D.; Borisov, A. P.; Semenenko, K. N. *Russ. J. Inorg. Chem.* **1986**, *31*, 908−910.
(91) Zange, E. *Chem. Ber.* **1960**, *93*, 652−657.
(92) Mirsaidov, U.; Shaimuradov, I. B.; Khikmatov, M. *Russ. J. Inorg. Chem.* **1986**, *31*, 753−754.
(93) Shaimuradov, I. B.; Badalov, A. B.; Marufi, V. I.; Mirsaidov, U. *Russ. J. Inorg. Chem.* **1991**, *36*, 773.
(94) Lobkovskii, É. B.; Kravchenko, S. E.; Kravchenko, O. V. *J. Struct. Chem. USSR* **1983**, *23*, 582−586.
(95) Shinomoto, R.; Zalkin, A.; Edelstein, N. M. *Inorg. Chim. Acta* **1987**, *139*, 97−101.
(96) Mirsaidov, U.; Rotenberg, T. G.; Dymova, T. N. *Dokl. Akad. Nauk Tadzh. SSR* **1976**, *19*, 30−33, ; Chem. Abstr. 85:136374.
(97) White, J. P. III; Deng, H.; Shore, S. G. *Inorg. Chem.* **1991**, *30*, 2337−2342.
(98) Keller, P. C. *Inorg. Chem.* **1971**, *10*, 2256−2259.
(99) Nöth, H.; Thomas, S. *Eur. J. Inorg. Chem.* **1999**, 1373−1379.
(100) Girolami, G. S.; Kim, D. Y.; Abelson, J. R.; Kumar, N.; Yang, Y.; Daly, S. U.S. Patent Appl. 59728, April 9, 2008.
(101) Kim, D. Y.; Girolami, G. S. *Inorg. Chem.* **2010**, *49*, 4942−4948.
(102) Daly, S. R.; Piccoli, P. M. B.; Schultz, A. J.; Todorova, T. K.; Gagliardi, L.; Girolami, G. *Angew. Chem., Int. Ed.* **2010**, *49*, 3379−3381.
(103) Daly, S. R.; Girolami, G. S. *Chem. Commun.* **2010**, *46*, 407−408.
(104) Daly, S. R.; Girolami, G. S. *Inorg. Chem.* **2010**, *49*, 5157−5166.
(105) Marks, T. J.; Kolb, J. R. *Chem. Rev.* **1977**, *77*, 263−293.
(106) Ephritikhine, M. *Chem. Rev.* **1997**, *97*, 2193−2242.
(107) Makhaev, V. D. *Russ. Chem. Rev.* **2000**, *69*, 727−746.
(108) Kumar, N.; Yanguas-Gil, A.; Daly, S. R.; Girolami, G. S.; Abelson, J. R. *Appl. Phys. Lett.* **2009**, *95*, 144107/1−144107/3.
(109) Daly, S. R.; Kim, D. Y.; Yang, Y.; Abelson, J. R.; Girolami, G. S. *J. Am. Chem. Soc.* **2010**, *132*, 2106−2107.
(110) See Kepert, D. L. *Inorganic Stereochemistry*; Springer-Verlag: Berlin, 1982; Inorganic Chemistry Concepts, Vol. *6*, section 11 C.
(111) Clark, R. J. H.; Lewis, J.; Machin, D. J.; Nyholm, R. S. *J. Chem. Soc.* **1963**, 379−387.
(112) Deacon, G. B.; Evans, D. J.; Junk, P. C. *Z. Anorg. Allg. Chem.* **2002**, *628*, 2033−2036.
(113) Shannon, R. D. *Acta Crystallogr., Sect. A* **1976**, *A32*, 751−767.
(114) Makhaev, V. D.; Borisov, A. P. *Russ. J. Inorg. Chem.* **1999**, *44*, 1411−1413.
(115) Daly, S. R.; Girolami, G. S. *Inorg. Chem.* **2010**, *49*, 4578−4585.
(116) Deng, D.; Zheng, X.; Qian, C.; Sun, J.; Zhang, L. *J. Organomet. Chem.* **1994**, *466*, 95−100.
(117) Neculai, D.; Roesky, H. W.; Neculai, A. M.; Magull, J.; Schmidt, H.-G.; Noltemeyer, M. *J. Organomet. Chem.* **2002**, *643*−*644*, 47−52.
(118) Schumann, H.; Keitsch, M. R.; Muhle, S. H. *Acta Crystallogr., Sect. C: Cryst. Struct. Commun.* **2000**, *C56*, 48−49.
(119) Barbier-Baudry, D.; Blacque, O.; Hafid, A.; Nyassi, A.; Sitzmann, H.; Visseaux, M. *Eur. J. Inorg. Chem.* **2000**, 2333−2336.
(120) Trifonov, A. A.; Skvortsov, G. G.; Lyubov, D. M.; Fukin, G. K.; Fedorova, E. A.; Bochkarev, M. N. *Russ. Chem. Bull.* **2005**, *54*, 2511−2518.
(121) Skvortsov, G. G.; Yakovenko, M. V.; Fukin, G. K.; Cherkasov, A. V.; Trifonov, A. A. *Russ. Chem. Bull.* **2007**, *56*, 1742−1748.
(122) Bonnet, F.; Visseaux, M.; Hafid, A.; Baudry-Barbier, D.; Kubicki, M. M.; Vigier, E. *Inorg. Chem. Commun.* **2007**, *10*, 690−694.
(123) Lobkovskii, É. B. *J. Struct. Chem. USSR* **1983**, *24*, 224−230.
(124) Segal, B. G.; Lippard, S. J. *Inorg. Chem.* **1978**, *17*, 844−850.
(125) Schumann, H.; Keitsch, M. R.; Demtschuk, J.; Muehle, S. *Z. Anorg. Allg. Chem.* **1998**, *624*, 1811−1818.
(126) Qian, C.-T.; Zou, G.; Nie, W.-L.; Sun, J.; Lemenovskii, D. A.; Borzov, M. V. *Polyhedron* **2000**, *19*, 1955−1959.
(127) Wang, H.; Wang, H.; Li, H.-W.; Xie, Z. *Organometallics* **2004**, *23*, 875−885.
(128) Robert, D.; Kondracka, M.; Okuda, J. *Dalton Trans.* **2008**, 2667−2669.
(129) Yuan, F.; Yang, J.; Xiong, L. *J. Organomet. Chem.* **2006**, *691*, 2534−2539.
(130) Yuan, F.; Zhu, Y.; Xiong, L. *J. Organomet. Chem.* **2006**, *691*, 3377−3382.
(131) Peters, J. A.; Huskens, J.; Raber, D. J. *Prog. Nucl. Magn. Reson. Spectrosc.* **1996**, *28*, 283−350.
(132) Bertini, I.; Turano, P.; Vila, A. J. *Chem. Rev.* **1993**, *93*, 2833−2932.
(133) Bleaney, B. *J. Magn. Reson.* **1972**, *8*, 91−100.
(134) Golding, R. M.; Halton, M. P. *Aust. J. Chem.* **1972**, *25*, 2577−2581.
(135) Golding, R. M.; Pyykko, P. *Mol. Phys.* **1973**, *26*, 1389−1396.
(136) Pinkerton, A. A.; Rossier, M.; Spiliadis, S. *J. Magn. Reson.* **1985**, *64*, 420−425.
(137) Reilley, C. N.; Good, B. W.; Allendoerfer, R. D. *Anal. Chem.* **1976**, *48*, 1446−1458.
(138) Elgavish, G. A.; Reuben, J. *J. Am. Chem. Soc.* **1977**, *99*, 5590−5591.
(139) Reuben, J.; Elgavish, G. A. *J. Magn. Reson.* **1980**, *39*, 421−430.
(140) Lanthanum was used to determine LIS values for the larger paramagnetic lanthanides Ce−Sm and lutetium was used to determine the LIS values for the smaller lanthanides Tb−Yb. The data for the samarium complex was excluded from the LIS plots using eqs 3 and 4 because it yielded poor linear regressions. Poor fits in LIS plots have been previously attributed to samarium complexes because of its very small ⟨*Sz*⟩ value (0.06). See: Ren, J.; Zhang, S.; Sherry, A. D.; Geraldes, C. F. G. C. *Inorg. Chim. Acta* **2002**, *339*, 273−282.
(141) Reuben, J. *J. Magn. Reson.* **1982**, *50*, 233−236.
(142) Geraldes, C. F. G. C.; Sherry, A. D.; Kiefer, G. E. *J. Magn. Reson.* **1992**, *97*, 290−304.
(143) Marques, M. P. M.; Geraldes, C. F. G. C.; Sherry, A. D.; Merbach, A. E.; Powell, H.; Pubanz, D.; Aime, S.; Botta, M. *J. Alloys Compd.* **1995**, *225*, 303−307.
(144) Forsberg, J. H.; Delaney, R. M.; Zhao, Q.; Harakas, G.; Chandran, R. *Inorg. Chem.* **1995**, *34*, 3705−3715.
(145) Ren, J.; Zhang, S.; Sherry, A. D.; Geraldes, C. F. G. C. *Inorg. Chim. Acta* **2002**, *339*, 273−282.
(146) Bag, P.; Floerke, U.; Nag, K. *Dalton Trans.* **2006**, 3236−3248.
(147) Ren, J.; Sherry, A. D. *J. Magn. Reson., Ser. B* **1996**, *111*, 178−182.
(148) Bernstein, E. R.; Hamilton, W. C.; Keiderling, T. A.; La Placa, S. J.; Lippard, S. J.; Mayerle, J. J. *Inorg. Chem.* **1972**, *11*, 3009−3016.
(149) Haaland, A.; Shorokhov, D. J.; Tutukin, A. V.; Volden, H. V.; Swang, O.; McGrady, G. S.; Kaltsoyannis, N.; Downs, A. J.; Tang, C. Y.; Turner, J. F. C. *Inorg. Chem.* **2002**, *41*, 6646−6655.

(150) Phillips, W. D.; Miller, H. C.; Muetterties, E. L. *J. Am. Chem. Soc.* **1959**, *81*, 4496−4500.
(151) Aspinall, H. C.; Black, J.; Dodd, I.; Harding, M. M.; Winkley, S. J. *J. Chem. Soc., Dalton Trans.* **1993**, 709−714.
(152) Thompson, M. K.; Lough, A. J.; White, A. J. P.; Williams, D. J.; Kahwa, I. A. *Inorg. Chem.* **2003**, *42*, 4828−4841.
(153) Lama, M.; Mamula, O.; Kottas, G. S.; Rizzo, F.; De Cola, L.; Nakamura, A.; Kuroda, R.; Stoeckli-Evans, H. *Chem.—Eur. J.* **2007**, *13*, 7358−7373.
(154) Brumaghim, J. L.; Priepot, J. G.; Girolami, G. S. *Organometallics* **1999**, *18*, 2139−2144.